

1 **The Gutenberg-Richter Relation may not hold for the Anthropogenic Seismicity**

2

3 **A. Kostoglou<sup>1</sup>, B. Orlecka-Sikora<sup>1</sup>, S. Lasocki<sup>1</sup>, and F. Tong<sup>1</sup>**

4

5 <sup>1</sup>Institute of Geophysics, Polish Academy of Sciences, Warsaw, Poland

6 Corresponding author: Anastasios Kostoglou ([tkostoglou@igf.edu.pl](mailto:tkostoglou@igf.edu.pl))

7

8 A. Kostoglou: 0000-0002-9217-3173

9 B. Orlecka-Sikora: 0000-0002-0182-1455

10 S. Lasocki: 0000-0002-3443-6473

11 F. Tong: 0000-0002-3849-884X

12

13

14 **Acknowledgements**

15 We would like to thank Olivier Lengline and Weiwei Shu for the access to the experimental data

16 from Shu et al. (2023) (<https://doi.org/10.25577/2023-SHU-JGR>). The work presented in this

17 paper was supported by the project DT-Geo funded by Horizon Europe under the grant

18 agreement No 101058129. The funder had no role in study design, data collection and analysis,

19 decision to publish or preparation of the manuscript. Administrative support, article publishing

20 charges, travel, and writing assistance were provided by Institute of Geophysics Polish Academy

21 of Sciences.

22

23 **Abstract**

24           The empirical Gutenberg-Richter (GR) relation corresponds to an exponential model of  
25 magnitude distribution, the most widely used in the probabilistic assessments of seismic hazard  
26 and related risk. However, due to the complexity of seismic processes induced by technological  
27 activities, this model may not be applicable to anthropogenic seismicity (AS). Applying statistical  
28 hypotheses testing procedures, we investigate 63 AS catalogs resulting from various  
29 anthropogenic activities such as reservoir impoundment, underground mining, conventional and  
30 unconventional hydrocarbon extraction, geothermal energy production, and underground gas  
31 storage. In 30 cases (47.6%) the exponential model for magnitude is rejected. Furthermore, in 16  
32 out of these cases, the magnitude probability density functions are complex, having either modes  
33 or bumps or both. We discuss possible reasons for the discovered statistically significant  
34 deviations of the actual magnitude distributions from the exponential distribution and hence  
35 from the GR relation. We demonstrate that using the exponential distribution may lead to  
36 unacceptable inaccuracy of seismic hazard estimates in AS. As a remedy, we recommend the use  
37 of kernel nonparametric estimators of magnitude distribution.

38

39

40 **Keywords**

41 Gutenberg–Richter relation breakdown, Statistical seismology, non-parametric estimation,  
42 anthropogenic seismicity

43

## 44 1. Introduction

45 The phenomenon of Anthropogenic Seismicity (AS) accompanying the energy and raw  
46 materials subsurface projects is well known (Grigoli et al., 2017; Foulger et al., 2018; Lasocki &  
47 Orlecka-Sikora, 2020). The socio-economic impacts of anthropogenic earthquakes are significant  
48 and can threaten or prohibit the development of the associated industries, including those  
49 promoted in the transition to the low-carbon future, such as geothermal energy production and  
50 CO<sub>2</sub> sequestration. Seismic hazard and related risk assessment are the crucial information to  
51 protect lives, livelihoods and critical infrastructure. Probabilistic Seismic Hazard Analysis (PSHA)  
52 is the basic method of seismic hazard assessment in areas of natural and anthropogenic  
53 seismicity. One of the key pieces of information for the PSHA is the Frequency-Magnitude  
54 Distribution (FMD). The FMD presents the proportions of magnitude intervals in a population of  
55 earthquakes. A model of this distribution has a fundamental impact on the results of the  
56 estimation of probabilistic characteristics of the seismic process. The FMD models used in  
57 seismology usually are derived from an empirical relationship known as the Gutenberg-Richter  
58 (GR) relationship (Gutenberg & Richter, 1944). This law relates linearly the logarithm of the  
59 number of earthquakes,  $N$ , in a region that are above a certain magnitude,  $M$ , as  $\log N = a -$   
60  $bM$ , with  $a$  being a constant characteristic of the seismogenic process in the region and  $b$  being  
61 the ratio of weaker to stronger earthquakes. High  $b$  values indicate a higher proportion of smaller  
62 to large earthquake magnitudes in contrast to the pattern observed with low  $b$  values. The GR  
63 relation approximates the linear part of FMD that begins above the magnitude of completeness,  
64  $M_c$  - the lowest magnitude of earthquakes, which are statistically all recorded in given monitoring

65 conditions. The GR relation leads to exponential models of magnitude distributions, either  
66 unlimited or with upper limits.

67 Deviations from the exponential Gutenberg–Richter (GR) distribution have long been  
68 observed in mining environments (Kijko et al. 1987; Subbaramu et al., 1989; Johnston and  
69 Einstein, 1990; Trifu et al., 1993; Feustel, 1997, Lasocki, 2001; Orlecka-Sikora & Lasocki, 2005;  
70 Lasocki & Orlecka-Sikora, 2008, Urban et al., 2016), often attributed to the coexistence of two  
71 types of events: those directly related to mining operations and those resulting from stress  
72 redistribution within the mine. Similar observation of deviations from the GR law have been  
73 made for seismicity triggered in the vicinity of reservoirs and were connected with mixing of  
74 samples with different b-values (Urban et al., 2016). In these settings, temporal variability in b-  
75 values has been documented prior to moderate events ( $M \sim 4$ ) (Mallika et al., 2013). In the context  
76 of hydraulic fracturing, small-magnitude earthquakes frequently deviate from the GR relation  
77 (Eaton et al., 2014; Huang and Beroza, 2015; Leptokarpoulos et al. 2020). A return to GR-like  
78 behaviour after injection has ceased has been interpreted as evidence of stress triggering (Huang  
79 and Beroza, 2015). Additionally, hydraulic fracturing may induce seismicity through fault  
80 reactivation, indicated by an increase in event magnitude over time and a concurrent drop in b-  
81 value (Davies et al., 2013). However, as Leptokarpoulos et al. (2020) point out, interpreting  
82 magnitude distributions solely based on b-value variations in such cases may be misleading when  
83 the underlying distribution deviates from exponentiality.

84 The multicomponent structure of the FMD in some anthropogenic seismicity cases were  
85 evidenced observationally and proved statistically (e.g. Gibowicz & Lasocki (2001) and references  
86 therein). Using the smoothed bootstrap test for multimodality (Silverman, 1986), Lasocki (2001)

87 validated statistically hypotheses on the multimodality of the FMD of mining earthquakes.  
88 Furthermore, he demonstrated that no parametric model of the FMD could fit such data to  
89 ensure the required accuracy of the FMD representation in the probabilistic PSHA. In studies of  
90 the FMD complexity for four the AS datasets from mine, geothermal energy production field and  
91 reservoir impoundment statistically significant non-exponentiality of the FMDs was found (Urban  
92 et al., 2016). **In this study, we generalize these findings and hypothesize that FMD not following**  
93 **the GR-born exponential distributions and often having a multimodal structure is a general**  
94 **feature of the FMD-s of the AS.** To get grounds on this hypothesis we investigate the FMD for  
95 the AS catalogues that result from the anthropogenic activities of a wide range of technological  
96 operations. We selected 18 AS episodes representing different impacting factors such as  
97 reservoir impoundment, underground mining, conventional and unconventional hydrocarbon  
98 extraction, geothermal energy production and underground gas storage from the datasets of the  
99 AS hosted by the EPISODES platform (Orlecka-Sikora et al., 2020; Lasocki et al., 2022) of the  
100 Thematic Core Service Anthropogenic Hazards (TCS AH), and developed within the European  
101 Plate Observing System Program (EPOS-ERIC). EPISODES Platform opens the unique opportunity  
102 for broad studies across technology of the AS by providing access to datasets called the episodes,  
103 which encapsulate the geological, geophysical and technological information. Our testing scheme  
104 is similar to that employed by Leptokaropoulos (2020) for his tests of the Geysers catalog. We  
105 examine the fit of the FMD of the AS to the GR relations using the parametric Anderson–Darling  
106 (AD) test (Stephens, 1974) for the exponential distribution. Subsequently, we examine the  
107 complexity of the FMD, searching for multiple modes and bumps in the Probability Density (PDF).  
108 For this purpose we employ the nonparametric smoothed bootstrap multimodality and

109 multibump tests (Silverman, 1986; Efron & Tibshirani, 1998) for the first time used to study  
110 magnitude distribution by Lasocki (2001). We find that among the 63 of the analyzed AS  
111 catalogues associated with various technological operations, in 30 cases (47.6%) the magnitude  
112 distribution deviates significantly from the GR-born distribution. Furthermore, in 16 out of these  
113 30 cases, (53.3%) the magnitude distribution is complex, with either more than one mode or  
114 more than one bump, or both. We discuss possible reasons of the found complexity of magnitude  
115 distribution. Finally, we recommend the use of the kernel nonparametric estimation of  
116 magnitude distribution in the probabilistic seismic hazard analysis of AS, proposed by Lasocki et  
117 al. (2000) and Kijko et al. (2001).

118

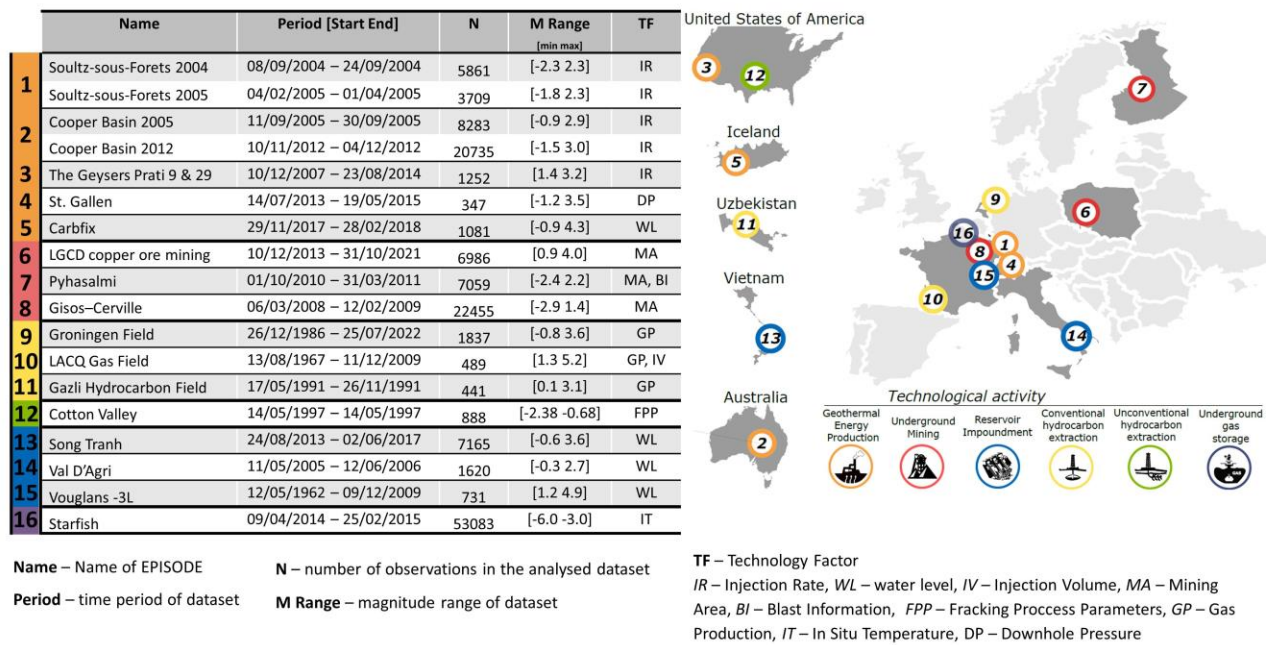
## 119 **2. Anthropogenic Seismicity Data and Methodology**

120

### 121 **2.1 Anthropogenic Seismicity Cases**

122 For the FMD testing procedure we select eighteen episodes representing AS categorized by  
123 the six different technological causative activities which can induce seismicity through various  
124 physical processes: **underground mining** where excavation leads to stress redistribution (e.g.  
125 Gibowicz and Kijko, 1994); **reservoir impoundment** which causes stress changes due to the filling  
126 of the reservoir and pore pressure changes due to diffusion (Lizurek et al., 2021 and references  
127 therein); **conventional and unconventional hydrocarbon extraction** where reservoir depletion  
128 leads to pore pressure reduction and associated stress changes (McGarr et al., 2002); **geothermal**  
129 **energy production** which affects subsurface stresses through both thermoelastic and poroelastic  
130 effects (Orlecka-Sikora et al., 2020 and references therein) and **underground gas storage** where  
131 triggering mechanisms include pore pressure buildup due to gas injection and potentially gas

132 buoyancy (Vilarrasa et al., 2021). The data is selected to ensure an abundance of seismological  
 133 observations required for the statistical inference. The basic available seismic information for  
 134 each episode is a seismic catalog along with the information about the associated seismic  
 135 network. The data are paired with industrial information such as injection rates for episodes  
 136 related to hydraulic fracturing, mining areas and mining front advance in episodes related to  
 137 underground mining, and water level changes for AS related to the reservoir impoundment. The  
 138 basic parameters of the studied episodes along with their location are presented in Fig. 1. The  
 139 detailed description of data with the associated references are provided in the Supplementary  
 140 Note 1.



141  
 142 **Figure 1. Information about the episodes from the EPISODES Platform of EPOS TCS AH, selected for the FMD**  
 143 **testing procedure:** time and magnitude range, number of earthquakes and value of the inducing technological  
 144 factor, along the episodes' geographical distribution.

145

146 Due to the specific properties of the AS, especially its dependence on spatial and temporal  
147 changes of technological processes inducing this seismicity (Lasocki & Orlecka-Sikora, 2020), the  
148 data selection is carried out according to an established scheme adapted to the AS  
149 characteristics. First, for each catalog we identify seismicity clusters based on the spatial and  
150 temporal evolution of the causative technological activity. This step results in the catalogs  
151 fragmentation into the smaller sub-catalogs. For seismicity related to fluid injection with a  
152 number of injection cycles we select the catalog according to those cycles and the temporal  
153 evolution of each injection cycle. For earthquakes induced by underground mining, based on the  
154 location of mining panels and mining front advance, if available, we extract the associated  
155 hypocentral distribution and then proceed to further processing. For the reservoir impoundment  
156 AS episodes, we relate datasets to the level of water in the reservoir. In the second step, we focus  
157 on the stationarity of the AS process in the selected catalogs and sub-catalogs.

158 Particular attention is devoted to the estimation of the magnitude completeness level,  $M_c$ ,  
159 as its improper estimation may provide spurious rejections of the exponentiality of the observed  
160 magnitude distributions. We use five tests to estimate the  $M_c$ : the Goodness of Fit test (Wiemer  
161 & Wyss, 2000) at the 90% (GFT90), and 95% (GFT95) level, the modified Goodness of Fit test  
162 (mGFT, Leptokaropoulos et al., 2013), the Maximum Curvature test (MaxCurv, Wiemer & Wyss,  
163 2000) and the MBASS test (Amorese, 2007). For every examined catalog we compare the results  
164 of the five tests and we found that the mGFT provides the highest or second highest value of  $M_c$   
165 in 51 of the 52 catalogs that we initially explored (Table A1). The GFT95 and MBASS methods also  
166 provide high  $M_c$  values but also sometimes they fail to calculate an  $M_c$ . Furthermore, the GFT95  
167 method provides in some cases unrealistic value for  $M_c$ , much higher than the values from other

168 methods (e.g. The Soultz-Sous-Forets 2005 injection) and is not taken into account. The GFT90  
169 method provides usually the lowest  $M_c$ -value and in two cases also fails to produce a result. The  
170 MaxCurv method provides low  $M_c$  estimate in FMDs with low curvature (e.g., Cooper Basin 2005  
171 and 2012, Starfish). Those observations lead us to use the mGFT test for our  $M_c$  estimations.

172       After determining the  $M_c$  for a catalog using the mGFT test, we assess its spatial variability.  
173 To achieve this, we divide the study area into an  $N \times N$  grid. Each grid cell must contain a minimum  
174 of 20 earthquakes to calculate a reliable  $M_c$  value. This threshold is chosen to balance sample  
175 size and spatial coverage, especially in cases with limited events. While low sample sizes may  
176 introduce slight biases, Gong et al. (2024) show that the GFT90 method performs reasonably well  
177 even with as few as 20 events. The mGFT method, being more conservative than GFT90, likely  
178 overestimates  $M_c$  slightly, providing a cautious estimate. The selection of  $N$  was determined  
179 empirically for each case to ensure that a sufficient number of events were retained for analysis.  
180 In most cases, some spatial variability in  $M_c$  is observed. However, this approach ensures that  
181 the overall calculated  $M_c$  is always equal to or greater than the highest  $M_c$  value within the grid.  
182 While this approach is precautionary, we maintained this criterion to avoid introducing potential  
183 biases in b-value or FMD model comparisons in marginal areas

184       In the next step, we focus on the stationarity of the AS process in the selected catalogs and  
185 sub-catalogs. The AS process is intrinsically non-stationary but usually can be regarded as interval  
186 stationary (Węglarczyk & Lasocki, 2009; Olszewska et al., 2017). We identify the stationary  
187 intervals, based on cumulative number of earthquakes with  $M \geq M_c$ , versus time plots. The linear  
188 parts of such plots indicate the constant seismicity rate. Before applying the statistical tests to  
189 detect deviations from exponential distribution and detect complexity, each stationary period is

190 examined with non-overlapping rolling windows of 60, 100, or 200 earthquakes, depending on  
191 catalog size. It is confirmed that that within each window, the estimated  $M_C$  does not exceed the  
192 overall calculated  $M_C$ .

193 The presented above methods of selecting the samples for the goodness of fit tests, in our  
194 opinion secured the study from the factors that might distort test results like over- or  
195 underrepresentation of lower magnitudes in catalogs (Herrman & Marzocchi, 2020) and  
196 incompleteness of catalog subsets (Marzocchi et al., 2020).

197 Finally, to ensure samples representativeness we accept the subcatalogs with minimum 60  
198 events above the  $M_C$ . Based on our evaluation of the statistical power of exponentiality tests  
199 (Supplementary Note 2.1), a sample size of at least 60 was identified as a reliable minimum  
200 threshold for detecting deviations from exponentiality using the Anderson-Darling (AD) test.  
201 Following this workflow, we determined 63 subsets containing altogether 22131 seismic events  
202 (Fig. 1, Supplementary Note 1).

203

## 204 **2.2 Testing scheme**

205 The deviation of the FMDs of the selected catalogs from the GR law and the complexity of  
206 the underlying magnitude distribution is explored with two approaches. First, the AD test  
207 (Anderson & Darling, 1954; Stephens, 1974) checks whether the tested sample is drawn from the  
208 exponential distribution with the  $b$  parameter estimated by the maximum likelihood method  
209 (Aki, 1965; Bender, 1983) – the  $H_0^1$  hypothesis, against the alternative that it is not drawn from  
210 an exponential distribution. Our studies of the power of the exponentiality tests: the  
211 Kolmogorov-Smirnov (KS) one-sample test (Slakter, 1965), the Lilliefors (LF) test (Lilliefors, 1967)

212 and the AD test, presented in the Supplementary Note 2.1, indicate the AD test as the most  
213 powerful. We use AD test at the significance level 0.05.

214 In the second step, the non-parametric smoothed bootstrap multimodality and multibump  
215 tests (Silverman, 1986; Efron & Tibshirani, 1998; Lasocki & Papadimitriou, 2006) are applied to  
216 datasets for which the  $H_0^1$  hypothesis is rejected by the AD test. The multimodality test's null  
217 hypothesis is that the PDF of magnitude is modeless ( $H_0^2$  hypothesis) with the alternative that  
218 the PDF has at least one mode to the right from the global maximum that is at the catalog  
219 completeness magnitude,  $M_c$ . The multibump test explores the null hypothesis,  $H_0^3$ , that the  
220 magnitude distribution does not have bumps. The existence of multiple modes or bumps  
221 suggests mixing of components in a dataset (Cox, 1966).

222 These non-parametric smoothed bootstrap tests serve as an independent and supplementary  
223 method for identifying the presence of features (modes and/or bumps) that may cause the AD  
224 test to reject the exponential model of magnitude. These features are often located in the ranges  
225 of larger magnitudes, poorly represented by not very big samples. The significance level of  
226 complexity tests is hard to assess in the smaller sample frequencies of higher magnitudes (Cox,  
227 1966). Moreover, unlike the AD test, the non-parametric smoothed bootstrap tests are not  
228 modified to improve performance in the distribution tails. For these reasons we use these two  
229 tests at the significance level 0.1. The details on all the applied tests are provided in  
230 Supplementary Note 2.2.

231 These three tests study continuous random variables, which means that they cannot be used  
232 when a sample contains repeated values. Magnitude is intrinsically a continuous random  
233 variable, but seismic catalogs have repeated magnitude values due to round-offs. This problem

234 is tackled by randomizing the reported magnitudes above the magnitude of completeness within  
235 their round-off interval,  $\delta M$ , using the proposed solution of Lasocki & Papadimitriou (2006):

$$236 \quad M_{rand} = F^{-1} \left\{ u \left[ F \left( M + \frac{\delta M}{2} \right) - F \left( M - \frac{\delta M}{2} \right) \right] + F \left( M - \frac{\delta M}{2} \right) \right\}, \quad (1)$$

237 where  $F$  is the CDF of the best fitted exponential distribution of magnitude,  $F^{-1}$  is its inverse  
238 function, and  $u$  is a random value from the uniform distribution (0,1). This relationship preserves  
239 the exponential properties of the magnitude PDF while incorporating randomness. In this work,  
240 the round-off of the reported magnitudes was 0.1. In order not to lose the values that passed to  
241 the  $[Mc - \delta M/2]$  interval, we reduce  $Mc$  by  $\delta M/2$ . Finally, we repeat the randomization and testing  
242 process ten thousand times, and take the p-value of the AD-test as the median of all ten thousand  
243 p-values.

244

### 245 **2.3 Example: testing the complexity of the FMD of the seismicity from the Cooper** 246 **Basin 2012 Episode.**

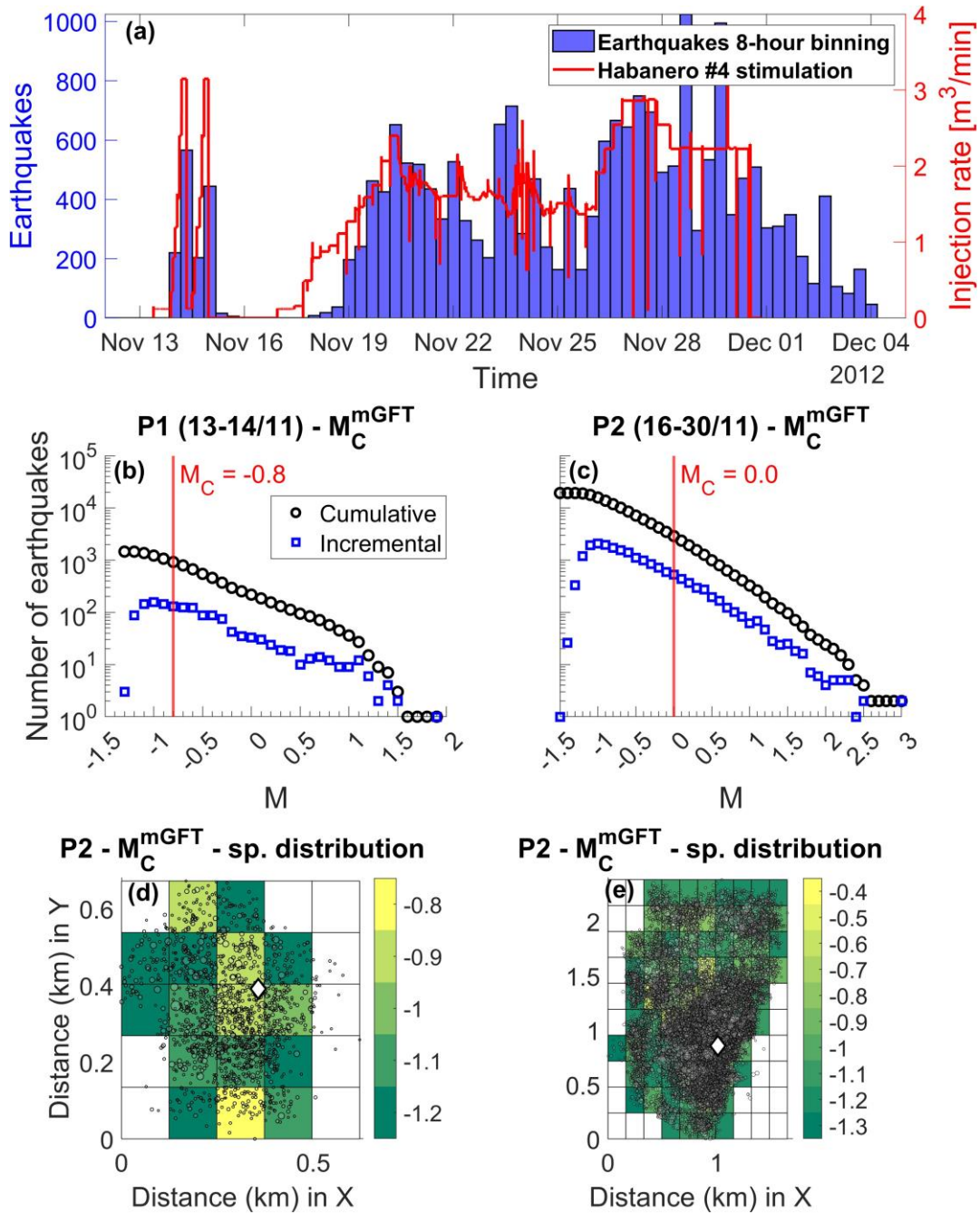
247 We present the testing process on the example of the Cooper Basin 2012 Episode's catalog.  
248 The Cooper Basin 2012 Episode contains the AS dataset associated with the geothermal energy  
249 production by hydraulic stimulation. The Cooper Basin geothermal field is located in the  
250 northeast of South Australia near the Queensland border. Geothermal exploration there started  
251 in 2002. The six deep wells were drilled into the granite to a depth level of 3629-4852 m. Four of  
252 these wells are located in the Habanero field, the other two wells are at distances of 9 and 18  
253 km, respectively, in the Jolokia and Savina fields. Several hydraulic stimulations were conducted  
254 to enhance the hydraulic conductivity in the subsurface. Stimulation activities in the Habanero

255 field were accompanied by intense seismic activity occurring on a single, subhorizontal fault  
256 (Baisch et al., 2006; 2009). A fluid-injection experiment was performed in the Habanero 1 well in  
257 2003 to stimulate a geothermal reservoir by 20000 m<sup>3</sup> of water injected into the granitic crust at  
258 4250 m depth. During reservoir stimulation about 27000 induced earthquakes were detected.  
259 High-resolution relative hypocenter locations confirmed that the reservoir is dominated by a  
260 single fracture zone. In September 2005, the Habanero 1 well was restimulated by injecting a  
261 total amount of 22500 m<sup>3</sup> of water into the 4421 m deep well. Maximum flow rates exceeded 31  
262 L/s and the wellhead pressure reached peak value of about 62 MPa. The Habanero 4 well was  
263 drilled in the year 2012 to a total depth of 4204 m. It intersects the previously stimulated  
264 reservoir at a depth level of 4160 m (Baisch et al., 2006; 2009; 2015). The Habanero 4 well was  
265 hydraulically stimulated by injecting 34 000 m<sup>3</sup> of water. Maximum flow rates exceeded 60 L/s,  
266 and the wellhead pressure reached peak values of about 50 MPa.

267 For monitoring the stimulation, a 24-station network was installed. The network includes the  
268 permanent stations installed around the Habanero, Jolokia, and Savina well sites, consisting of  
269 three-component geophones deployed in boreholes at depth levels of 78-370 m and one surface  
270 seismometer (Baisch et al., 2015). Additionally, nine stations equipped with three-component 1  
271 Hz surface seismometers were temporarily deployed to improve the coverage to the east and  
272 northwest, respectively. Each seismic station was equipped with a three-channel 24-bit digitizer  
273 recording continuously at a sampling rate of 500 Hz. The detailed description of the episode and  
274 the seismic data enriched with the injection rate for Habanero 1 and 4 wells, the drillhole  
275 trajectory of the wells, the position of the wells in the Cooper Basin geothermal field, time series

276 of wellhead pressure from for wells, seismic velocity model, and the geological map of the Cooper  
277 Basin site can be found on the EPISODES Platform (IS EPOS, 2020).

278 We inspect initially the number of earthquakes in relation to the injection rate and identify  
279 two periods of injection followed by a slightly delayed seismic response. These periods refer to  
280 an initial injection period before the main injection between 13 and 14 November 2012 and a  
281 main injection cycle between 16 and 30 November of 2012 (Fig. 2a). Seismicity is related to a  
282 single pre-existing surface (Baisch et al., 2009; 2015) and therefore we define clusters only by  
283 investigating the earthquake epicentral distribution. In the first injection period (P1) we define  
284 one cluster around the injection well (Fig. 2d; 3a) while in the second (P2) we identify the  
285 migration of seismicity away from the injection well (Fig. 2e; 3b).



286

287

288

289

290

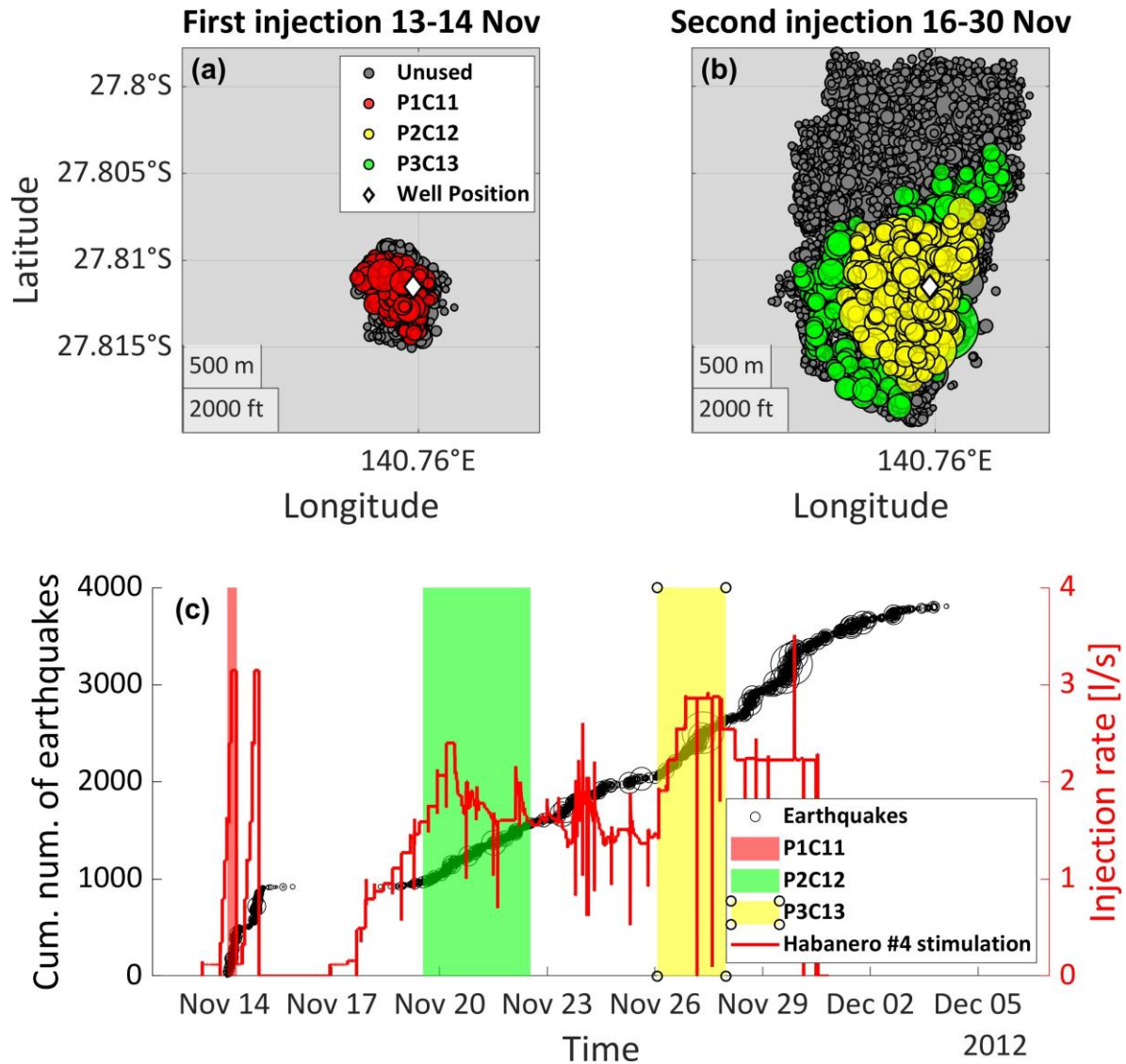
291

292

**Figure 2. Investigation of seismicity along with causative technology (inj. rate) and  $M_C$  calculation of the Cooper Basin 2012 Episode** a. Seismic activity per 8 hours along with injection rate (top), b. estimation of the magnitude of completeness with the mGFT method (Leptokaropoulos et al., 2013) for the 1<sup>st</sup> injection period, P1 (Nov 13 – Nov 14) and, c. for the second injection period, P2 (Nov 16 – Nov 30), d. spatial distribution of the magnitude of completeness over a gridded area for the 1<sup>st</sup> injection period, P1 and e. for the second injection period, P2. The injection well is represented by the white diamond and the earthquake epicenters by circles in d and e.

293 In the next step, we estimate an  $M_C$  of  $-0.8$  for the first injection period and an  $M_C$  of  $0.0$  for  
294 the second (Fig. 2b-c). To assess the spatial variability of  $M_C$ , we applied a  $5 \times 5$  grid for the first  
295 injection period and a  $10 \times 10$  grid for the second. During the first injection period (Fig. 2d),  $M_C$   
296 values range from  $-1.2$  to  $-0.8$ , confirming that the calculated value of  $-0.8$  for the entire area is  
297 appropriate. For the second injection period,  $M_C$  values across the grid vary between  $-1.3$  and  $-$   
298  $0.4$  (Fig. 2e), demonstrating that the overall  $M_C$  calculation of  $0.0$  using the mGFT method  
299 adequately accounts for spatial variability. We proceed to analyze the seismic activity in the  
300 selected clusters. We identify one stationary period for the P1 period, P1C11 (Fig. 3a; 3c-red  
301 color), and two stationary periods for the main injection period P2, P2C12 and P3C13 (Fig. 3b-c-  
302 yellow and green colors). As a final result we receive the three samples.

303



304

305

306

307

308

309

310

311

312

**Figure 3. Spatial and temporal distribution of stationary periods** a. epicentral distribution of earthquakes for the first injection period and b. for the second injection period. Colored circles represent the clusters that were chosen for analysis based on (c) while gray circles represent earthquakes that were not used in the final analysis. c. Identification of the seismicity stationary periods. The identified stationary periods are colored with the same colors that are used on the epicentral maps

After this step the exponentiality of magnitude distribution is tested. The results are summarized in Table 1. The exponentiality of the distribution can be rejected for the first (P1C11)

313 and third sample (P3C13) as the  $p$ -values of the AD test ( $H_0^1$ ) are below 0.05. The multimodality  
314 test does not indicate modes of magnitude density in both P1C11 and P3C13 ( $H_0^2 > 0.1$ ) but the  
315 magnitude density of the data from P3C13 very likely has bumps. Therefore, the complexity of  
316 the magnitude distributions is ascertained only for P3C13.

317 The step-by-step procedure for selecting appropriate subcatalogs, as presented for the  
318 Cooper 2012 episode catalog, is similarly applied to each of the selected EPISODES catalogs and  
319 detailed in Supplementary Note 1 (Figs. S1–S86).

320

### 321 **3. Results**

322

#### 323 **3.1. Geothermal energy production**

324 Following the procedure described above we determine fourteen clusters from the eight  
325 geothermal energy production episodes from the Soultz-sous-Forêts stimulation in France, from  
326 the Carbfix Reykjavík Energy Episode with geothermal energy production and CCS (Carbon  
327 Capture and Storage) - one of the most successful examples of CO<sub>2</sub> sequestration processes in  
328 the world, from Sankt Gallen experiment in Switzerland, from The Geysers geothermal field in  
329 USA - one of the largest geothermal fields worldwide, and from the mentioned above Cooper  
330 Basin Episode in Australia (Supplementary Note 1). The selected clusters from each episode that  
331 were analyzed contain between 76 and 3186 earthquakes, with magnitudes ranging from -1.6 to  
332 3.5. In seven clusters (50% of the considered datasets), the exponentiality of magnitude  
333 distribution is rejected (Table 1). Out of these seven samples, the complexity of the magnitude

334 distribution in the form of the presence either modes or inflections in the density function is  
 335 confirmed in three cases.

336

337 **Table 1. Significance of the hypotheses of the exponentiality and the complexity of the FMD of earthquakes in the**  
 338 **clusters from the seismicity episodes related to the geothermal energy production available on the EPISODES**  
 339 **Platform.** Statistically significant  $p$  values of Anderson-Darling ( $H_0^1$ ) and the non-parametric smoothed bootstrap  
 340 multimodality ( $H_0^2$ ) and multibump ( $H_0^3$ ) tests are highlighted in bold. The type of magnitude is provided next to the  
 341 EPISODE name

Episode Cluster	Number of earthquakes	Range of Magnitudes	$p$ value of the significance of the Hypothesis:		
			$H_0^1$	$H_0^2$	$H_0^3$
Cooper Basin 2005 ( $M_L$ )					
P1C1	1031	-0.2 – 2.9	<b>0.0005</b>	0.160	<b>0.040</b>
P2C1	686	-0.2 – 2.3	<b>0.0477</b>	0.257	0.575
P3C1	803	-0.2 – 2.4	<b>0.0158</b>	0.355	0.403
P4C2	208	-0.3 – 1.3	0.2086	-	-
P5C2	206	-0.3 – 2.2	0.4529	-	-
Cooper Basin 2012 ( $M_L$ )					
P1C11	503	-0.8 – 0.5	<b>0.0213</b>	0.781	0.893
P2C12	3186	0.0 – 2.3	0.1482	-	-
P3C13	2855	0.0 – 3.0	<b>0.0464</b>	0.215	<b>0.092</b>
The Geyshears ( $M_w$ )					
P1C11	108	2.0 – 2.9	0.3059	-	-
Soultz-sous-Forêts 2004 ( $M_L$ )					
P1C1	532	0.3 – 2.3	<b>0.0117</b>	0.119	0.335
Soultz-sous-Forêts 2005 ( $M_L$ )					
P1C1	721	-0.4 – 2.3	<b>0.0098</b>	<b>0.043</b>	<b>0.030</b>
Carbfix ( $M_L$ )					
P1C1	108	0.8 – 2.3	0.3059	-	-
P2C2	76	0.9 – 2.0	0.1048	-	-
Sankt Gallen ( $M_L$ )					
P1C1	174	-0.6 – 3.5	0.6048	-	-

342 **3.2. Underground mining**

343 We use three episodes from the EPISODES Platform. These are the GISOS–CERVILLE Solution  
 344 Mining in France and two cases of underground hard rock mining: the Legnica-Glogow Copper  
 345 District (LGCD) in Poland, and the Pyhäsalmi Mine in Finland. We examine the FMD of 24 spatio-  
 346 temporal clusters from these three episodes. The number of events in the clusters ranges from  
 347 67 to 551 and magnitudes range is from -1.0 to 4.0 (Table 2; Supplementary Note 1). The  
 348 exponential distribution of magnitudes is rejected for fifteen clusters (62.5%). From those fifteen  
 349 cases, in seven cases the statistical tests signify the complexity of magnitude distribution.

350

351 **Table 2. Significance of the hypotheses of the exponentiality and the complexity of the FMD of earthquakes in the**  
 352 **clusters from the seismicity episodes related to mining exploitation available on the EPISODES Platform.**

353 Statistically significant *p* values of Anderson-Darling ( $H_0^1$ ) and the non-parametric smoothed bootstrap  
 354 multimodality ( $H_0^2$ ) and multibump ( $H_0^3$ ) tests are highlighted in bold. The type of magnitude is provided next to the  
 355 EPISODE name.

Episode Cluster	Number of earthquakes	Range of Magnitudes	<i>p</i> value of the significance of the Hypothesis:		
			$H_0^1$	$H_0^2$	$H_0^3$
LGCD ( $M_w$ )					
P1C1	146	2.1 – 3.2	0.6210	-	-
P1C2	136	1.9 – 2.9	0.1200	-	-
P2C2	125	1.9 – 3.0	0.0807	-	-
P1C4	79	1.8 – 3.3	<b>0.0311</b>	0.241	0.493
P1C5	84	1.5 – 3.7	<b>0.0185</b>	0.223	0.383
P1C6	73	1.7 – 3.6	0.0860	-	-
P2C6	90	1.7 – 2.9	<b>0.0085</b>	0.710	0.608
P3C6	87	1.7 – 3.5	0.7331	-	-
P1C7	89	1.7 – 3.7	0.1350	-	-
P2C7	67	1.7 – 3.9	<b>0.0247</b>	0.281	0.661
P1C8	82	1.7 – 3.3	0.3580	-	-
P2C8	165	1.7 – 3.4	<b>0.0107</b>	0.416	0.573
P1C9	94	1.9 – 4.0	<b>0.0147</b>	<b>0.024</b>	<b>0.042</b>
P1C10	86	1.8 – 3.5	<b>0.0410</b>	0.859	0.887

P2C10	86	1.8 – 3.3	0.3813	-	-
Pyhasalmi (M <sub>L</sub> )					
P1C1	212	-0.9 – 0.2	<b>0.0228</b>	0.112	0.199
P2C1	127	-0.9 – 1.1	<b>0.0058</b>	<b>0.010</b>	<b>0.010</b>
P1C2	70	-1.0 – -0.1	<b>0.0340</b>	<b>0.059</b>	0.897
P2C2	150	-1.0 – 1.2	<b>0.0380</b>	<b>0.010</b>	<b>0.010</b>
P3C2	149	-1.0 – 0.0	<b>0.0370</b>	<b>0.029</b>	0.897
Gisos–Cerville (M <sub>w</sub> )					
P1C1	541	-0.7 – 1.0	<b>0.0172</b>	<b>0.060</b>	0.114
P2C1	547	-0.7 – 1.0	<b>0.0302</b>	<b>0.099</b>	0.194
P3C1	185	-0.7 – 1.4	0.1293	-	-
P4C1	551	-0.7 – 1.3	<b>0.0085</b>	0.467	0.917

### 3.3 Reservoir Impoundment.

The catalogs related to the reservoir impoundment are represented by three episodes from the Song-Tranh reservoir in Vietnam, the Val d’ Agri reservoir in Italy, and the Vouglans reservoir in France. The clusters in the area of the Song-Tranh reservoir are adopted from Lizurek et al. (2017) and Orlecka-Sikora et al.(2023). We examine the seismicity clusters close to the reservoir Val d’Agri after Valoroso et al. (2009). In case of the Vouglans reservoir, we select the earthquake cluster around the area of the reservoir. The identify eight clusters contain from 75 to 249 earthquakes, with magnitudes from 0.2 to 3.3 (Table 3). The AD test rejects the FMD exponentiality of magnitude distribution for one cluster, from the Val d’Agri area. The complexity tests do not provide grounds to reject the hypotheses  $H_0^2$  and  $H_0^3$ .

### 3.4 Conventional and unconventional hydrocarbon extraction, underground gas storage.

We investigate five episodes related to the exploitation of underground reservoirs. The Cotton Valley episode describes the seismic process associated with the unconventional hydrocarbon extraction (Rutledge, 2004; IS EPOS, 2019). The three conventional hydrocarbon

372 extraction episodes examined here are the Groningen field, the LACQ field and the Gazli field.  
373 The Groningen gas field is a giant natural gas field located near Slochteren in Groningen province  
374 in the Netherlands. It has been discovered in 1959 and nowadays it is the largest natural gas field  
375 in Europe and one of the largest in the world. The analyzed catalog contains the data of seismicity  
376 since the end of 1986 with the local magnitude range,  $M_L$ , from -0.8 to 3.6. The Gazli field episode  
377 is related to the gas extraction in the area of Gazli in Uzbekistan (Plotnikova et al., 1996; Adushkin  
378 et al., 2016). The catalog contains the seismic data from 1976 to 2015. For the FMD exponentiality  
379 and complexity tests we select a catalog from a local experiment in 1991, with  $M_w$  range from  
380 0.1 to 3.1. The LACQ field episode is related to a seismic swarm in the vicinity of a deep  
381 conventional gas extraction in Aquitaine, France. Due to the changes in the seismic network in  
382 LACQ, we establish two periods (pre and after 1996) with different levels of magnitude  
383 completeness. The last episode in this group is the Starfish experiment undertaken in an  
384 underground salt mine in Grand Est, France to assess the influence of thermal loading of high-  
385 frequency gas storage operations cycles on the stability of salt cavities. This episode contains  
386 acoustic emission data with magnitudes between -6.0 and -3.0 related to four heating cycles. In  
387 the present group of AS, we identify seventeen clusters with 64 to 953 earthquakes of  
388 magnitudes from -4.8 to 3.7. The statistical test rejects the exponential distribution of  
389 magnitudes in seven clusters (41.2%). The complexity of the magnitude distribution is  
390 ascertained in six cases (Table 3).

391

392 **Table 3. Significance of the hypotheses of the exponentiality and the complexity of the FMD of earthquakes in the**  
393 **clusters from the seismicity episodes related to the reservoir impoundment, the conventional and unconventional**  
394 **hydrocarbon extraction, underground gas storage, available on the EPISODES Platform.** Statistically significant  $p$

395 values of Anderson-Darling ( $H_0^1$ ) and the non-parametric smoothed bootstrap multimodality ( $H_0^2$ ) and multibump  
 396 ( $H_0^3$ ) tests are highlighted in bold. The type of magnitude is provided next to the EPISODE name.

Episode Cluster	Number of earthquakes	Range of Magnitudes	$p$ value of the significance of the Hypothesis:		
			$H_0^1$	$H_0^2$	$H_0^3$
<b>Reservoir Impoundment</b>					
Song – Tranh 2 ( $M_L$ )					
P1C1	200	0.9 – 3.2	0.2750	-	-
P2C2	249	1.0 – 3.3	0.4498	-	-
P3C3	122	0.8 – 2.0	0.2704	-	-
Val d' Agri ( $M_L$ )					
P1C1	159	0.2 – 2.1	<b>0.0168</b>	0.459	0.674
P2C1	75	0.2 – 2.1	0.4065	-	-
P2C2	85	0.2 – 1.7	0.1650	-	-
P4C1	200	0.2 – 2.7	0.4247	-	-
Vouglans ( $M_w$ )					
P1C1	138	1.8 – 3.0	0.1300	-	-
<b>Conventional Hydrocarbon Extraction</b>					
LACQ ( $M_w$ )					
P1C1	108	2.2 – 3.7	0.1270	-	-
P2C1	125	1.8 – 3.4	0.1955	-	-
P3C1	63	1.8 – 3.0	0.0864	-	-
Groningen ( $M_w$ )					
P1C1	123	1.2 – 3.5	0.7866	-	-
P2C1	175	0.9 – 3.6	0.2163	-	-
P3C1	70	0.6 – 2.3	0.1348	-	-
P4C1	118	0.6 – 3.4	0.4529	-	-
Gazli 1991 ( $M_w$ )					
P1C1	129	0.8 – 2.7	0.3385	-	-
<b>Unconventional Hydrocarbon Extraction</b>					
Cotton Valley ( $M_w$ )					
P1C1	68	-2.0 – -1.4	0.4569	-	-
P2C1	217	-2.0 – -0.7	<b>0.0096</b>	<b>0.030</b>	<b>0.018</b>
P3C1	64	-2.0 – -1.4	<b>0.0022</b>	<b>0.008</b>	<b>0.039</b>
<b>Underground Gas Storage</b>					
Starfish ( $M_L$ )					
P1C11	359	-4.2 – -3.4	<b>0.0006</b>	<b>0.005</b>	0.260
P1C12	282	-4.3 – -3.0	<b>0.0051</b>	0.359	0.693
P2C1	953	-4.6 – -3.5	<b>0.0005</b>	<b>0.012</b>	0.267
P3C1	697	-4.8 – -3.4	<b>0.0005</b>	<b>0.033</b>	<b>0.040</b>
P4C11	853	-4.7 – -3.3	<b>0.0005</b>	<b>0.002</b>	0.726

397	P4C12	434	-4.6 – -3.7	0.1507	-	-
-----	-------	-----	-------------	--------	---	---

398

399 **4. Discussion**

400 We found that among the 63 of the analyzed FMDs of AS associated with various technological  
401 operations, 30 (47.6%) reveal non-exponential underlying distribution. From these 30 of FMDs,  
402 16 show distribution complexity, with either modes or bumps, or both.

403 The AS process varies in time and space. The significant deviations of AS FMD-s from the GR  
404 based models can result from this variety and indirectly from diversity of technological factors  
405 inducing or triggering anthropogenic earthquakes and transient responses to the surrounding  
406 tectonic environment. The technological processes related to energy and raw materials geo-  
407 projects are often complex, liable to vary and change. They involve many various technological  
408 factors at the same time, e.g. fluid pressure, fluid injection rate, number of active injection and  
409 production wells etc., or e.g. amount of exploited ore, rate of mining, type of mining methods –  
410 longwall, room and pillar mining, block caving, and further, stress concentrations due to gob area,  
411 etc. The situation becomes even more complex in the cases where such projects are carried out  
412 in the vicinity of the fault systems that are heterogeneric and complex (e.g., Styles et al. (2014)).

413 Deviations of magnitude distributions from the exponential distribution were also discovered  
414 in natural seismicity. The applicability of the GR law is suggested to depend on the study area  
415 being sufficiently large, not only exceeding the source dimensions of the largest expected  
416 earthquake but also broad enough to encompass complex and variably oriented fault systems,  
417 ensuring the statistical validity of the G–R relationship (Krushelnitskii et al., 2024; Shebalin et al.,  
418 2024). An appropriate spatiotemporal scale should be large enough to reflect the tectonic

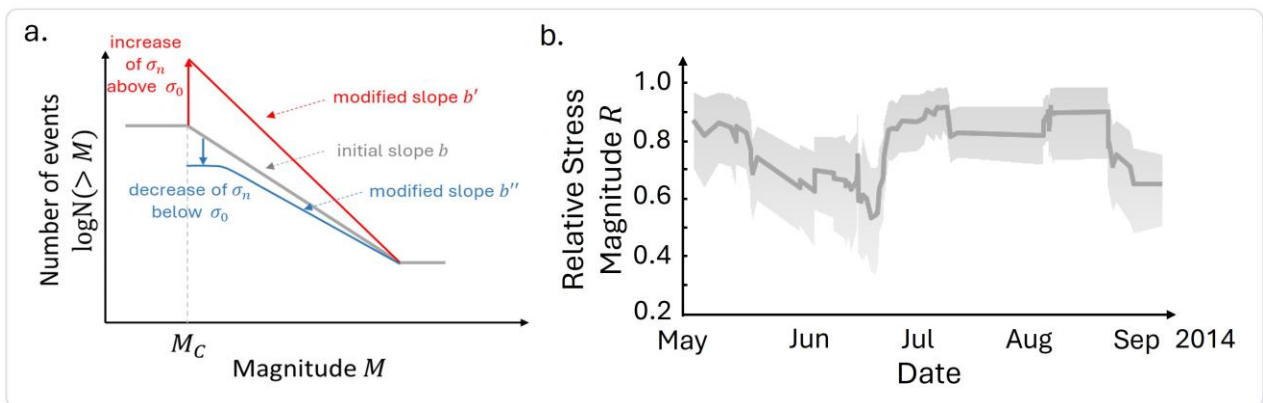
419 context without merging distinct FMD behaviors from different  $b$ -values, yet fine enough to  
420 preserve statistical validity (e.g. Herrmann et al., 2022). Therefore, it was recommended to use  
421 in the FMD studies a spatiotemporal selection of the high quality data above the catalogue  
422 completeness (Herrmann et al., 2022; Geffers et al., 2022) with proper sample sizes and  
423 magnitude ranges, typically of three units of magnitude (Marzocchi & Sandri, 2003), and the use  
424 of moment magnitudes,  $M_w$ , instead of local magnitudes,  $M_L$  (Herrmann & Marzocchi, 2021).  
425 Ideally,  $M_w$  would be calculated directly from the seismic signal though it is not always possible  
426 in the catalogs provided by the EPISODES platform. In these catalogs,  $M_w$  values sometimes may  
427 be derived from  $M_L$ , where the relationship between  $M_w$  and  $M_L$  is segmented polynomial  
428 (Goertz-Allmann et al., 2011; Edwards & Douglas, 2015). Our analysis indicates that  $M_L$  catalogs  
429 generally maintain the linearity for  $M \geq M_c$ , at smaller magnitudes, consistent with findings by  
430 Bethmann et al., (2011) and Deichmann (2017). The trend holds for the majority of our  $M_L$  based  
431 catalogs, except for the Song Tranh 2, Carbfix and St. Gallen episodes, which include maximum  
432 magnitudes above  $M_L 3.0$  but contain very few events above this magnitude (Tables 1; 2; 3).

433 Similar explanations of the non-exponentiality of magnitude distribution can also be found for  
434 AS cases. E.g., Igonin, et al. (2018) interpreted the observed bilinear magnitude distribution of  
435 the hydraulic fracturing-induced earthquakes close to Fox Creek, Alberta in Canada, as the result  
436 of the superposition of spatial clusters with different  $b$  values.

#### 437 **4.1 Mixtures of exponential distributions**

438 Dublanchet (2020) has shown theoretically and through numerical simulations that  $b$  value  
439 variations are related to normal stress observed in a mechanical model of fault, consisting of a  
440 frictional interface between elastic slabs, characterized by a heterogeneous distribution of critical

441 slip distance of the rate-and-state friction law. He has shown that  $b$  value increases with the  
 442 logarithm of normal stress as presented in the schematic diagram in Fig. 4a. According to  
 443 Dublanchet (2020) considerations, the FMD at the initial normal stress  $\sigma_n = \sigma_0$ , is characterized  
 444 by an exponent  $b$  (black line in Fig. 4a). Because of variations in  $\sigma_n$ , we observe changes in the  $b$   
 445 value from  $b$  to  $b'$  or from  $b$  to  $b''$  (marked by red and blue in Fig. 4a). In the case of AS, the rate  
 446 of stress changes due to the technological operations is high and the amplitudes of these changes  
 447 are significant. Such stress changes evolution for the AS case can be observed in Fig. 4b showing  
 448 the variations of the relative stress magnitude  $R = (\sigma_1 - \sigma_2)/(\sigma_1 - \sigma_3)$ , where  $\sigma_1, \sigma_2, \sigma_3$  are the  
 449 principal stresses, for the cluster of seismicity induced by the reservoir impoundment in the Song  
 450 Tranh 2 (ST2) reservoir in Vietnam (Orlecka-Sikora et al, 2023). The magnitudes of AS are  
 451 generated under nonstationary stress conditions, i.e., in the extreme case each of the magnitude  
 452 could represent the random variable coming from an exponential distribution of a different  
 453 exponent according to the inference of Dublanchet (2020). Thus, the use of the GR-based  
 454 distribution with one specific  $b$  value to model the FMD of the AS dataset covering a timespan of  
 455 the technological operation is questionable.



456  
 457 **Figure 4. a. Schematic representation of how changes in normal stress,  $\sigma_n$ , affect the slope (b-value) of the**  
 458 **frequency-magnitude distribution (FMD), adapted from Dublanchet (2020). The black solid line represents the**

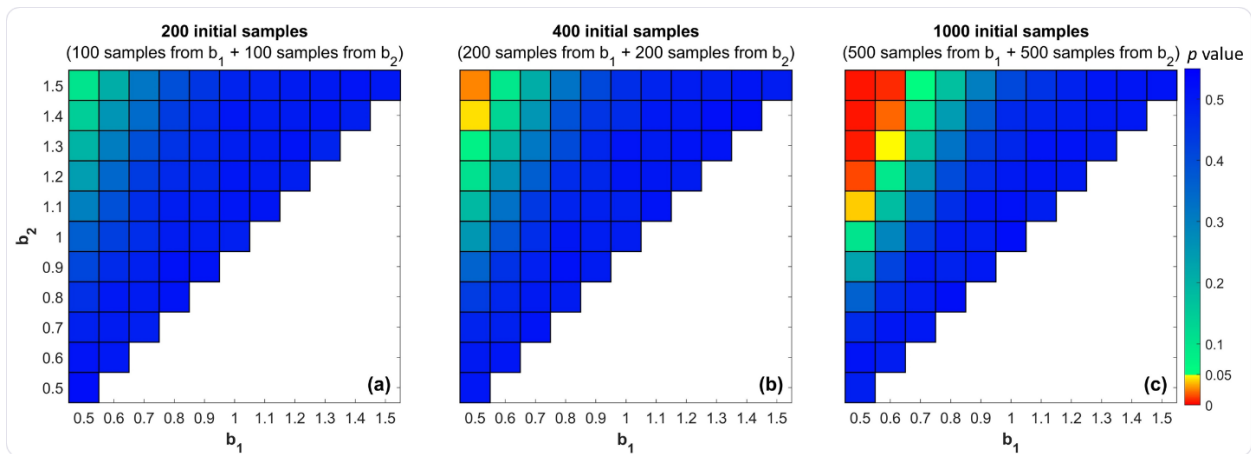
459 initial FMD, with  $b$ -value  $b$ ; increases or decreases in stress lead to modified slopes  $b'$  and  $b''$ . **b** Empirical example  
460 illustrating the evolution of relative stress magnitude  $R=(\sigma_1-\sigma_2)/(\sigma_1-\sigma_3)$ , where  $\sigma_1$ ,  $\sigma_2$  and  $\sigma_3$  are the principal  
461 stresses, over time for anthropogenic seismicity near the Song Tranh 2 reservoir in Vietnam. The gray shaded areas  
462 are the 95% confidence intervals. The variability in  $R$  supports the dynamic stress conditions hypothesized in panel  
463 (a), demonstrating the relevance of the schematic model to real AS cases.

464

465         Indeed, a mixture of exponential distributions with different exponents can, under  
466 specific conditions, produce a distribution whose complexity will be detected by goodness-of-fit  
467 tests. However, mixtures of the exponential distribution are monotone (Jewell, 1982; Heckman  
468 1990), that is the PDF cannot exhibit modality. In about half of our cases (16 cases) in which the  
469 null hypothesis  $H_0^1$  was rejected, the probability density complexity was also ascertained. The  
470 disparities between them and the GR-born exponential distribution could not result from the  
471 mixing of samples drawn from exponential distributions of different  $b$  values. However, in the  
472 second group of 14 cases, the modality was not confirmed; hence, the hypothesis that the results  
473 of the AD test were related to the mixture of the exponential distributions was not discarded.

474         To get insight into whether the observed FMDs are exponential mixtures or not we perform  
475 Monte Carlo simulations. We generate samples of 100, 200 and 500 magnitudes drawn from  
476 exponential distributions of various  $b$  values from 0.5 to 1.5. Then, we mix the samples with  
477 different exponentials in equal proportions (50% from each  $b$ -value), to create combined  
478 distributions of 200, 400 and 1000 samples that representing all possible combinations of  $b$ -  
479 values. The proportion is selected based on the real observations of  $b$  value time variations in AS  
480 clusters, where we observe that in most of the datasets about 50% of time periods experience  
481 lower values of  $b$  and 50% have higher values of  $b$  (the Supplementary Note 3). The results of

482 tests for the 200, 400 and 1000 element samples are presented in Fig. 5. We see that the  
 483 exponentiality of distribution is rejected only when the mixed sample is big (400 and 1000  
 484 elements) and it consists of data from two exponential distributions with strongly different  $b$ -  
 485 values (0.5 and  $\geq 1.4$  for 400 element samples, and 0.5 and  $\geq 1.1$  or 0.6 and  $\geq 1.3$  for 1000 element  
 486 samples).



487  
 488 **Figure 5. The results of the AD testing the hypothesis of exponentiality of the distribution gathered from the**  
 489 **mixture of the two exponential distributions with  $b_1$  and  $b_2$  parameters.** Panels show results for **a** 200, **b** 400, and  
 490 **c** 1000 samples, with each dataset composed of equal proportions from  $b_1$  and  $b_2$ .

491  
 492 To see whether such big changes of  $b$ -value occur in AS, we segment the original data in AS  
 493 clusters into 60-earthquakes of non-overlapping, consecutive subclusters and calculate the  $b$   
 494 value for these subclusters. The number of earthquakes in the subclusters is selected as a  
 495 compromise between the test power requirements and the need to observe the largest  $b$   
 496 variations. The  $b$ -value varies in the subclusters. The range of differences between  $b$ -values from  
 497 particular clusters is from 0.01 to 0.97 (the Supplementary Note 3.1, Fig. S90–S93). According to  
 498 the results presented in Fig. 5, these  $b$  variations for most of the sample sizes of AS subclusters  
 499 would not cause rejection of the null hypothesis by the AD test. Nevertheless, for many AS-tested

500 datasets with sample size below 400, the AD test rejected the hypothesis of an exponential  
501 distribution of magnitude. This indicates that the ascertained non-exponentiality of the AS FMDs  
502 does not result from the mixing of samples drawn from different exponential distributions.

503

#### 504 **4.2 Geological and technological constraints**

505 One possible mechanism responsible for the complex magnitude distribution is localized  
506 geological control. In many anthropogenic environments, seismicity occurs in highly confined  
507 zones influenced by specific stratigraphic layers, lithological contrasts, or fault structures. These  
508 features may concentrate stress and facilitate repeated rupture of similar size, reminiscent of the  
509 characteristic earthquake hypothesis proposed for natural tectonic systems (e.g., Wesnousky,  
510 1994). Under such conditions, the seismogenic volume in case of anthropogenic seismicity is  
511 limited by geology and by engineered interventions, which can further confine rupture sizes and  
512 stress accumulation patterns. Repetitive technological operations such as cyclic fluid injection,  
513 pressure drops, or mining step advances can introduce artificial loading patterns that repeatedly  
514 induce earthquakes within narrow magnitude bands. These operational thresholds or activation  
515 conditions may lead to pseudo-modal behavior in the magnitude distribution. It is also important  
516 to emphasize that the exploitation of georesources is typically managed to maintain seismic risk  
517 below an acceptable threshold. As part of this risk mitigation strategy, operators often adjust  
518 technological parameters (e.g., fluid injection schedules or extraction rates, Kwiatek et al., 2019)  
519 in response to the observed seismicity development, thereby intentionally suppressing the  
520 occurrence of larger-magnitude events. These interventions may further influence the resulting  
521 FMDs by altering the underlying stress regime and energy release dynamics.

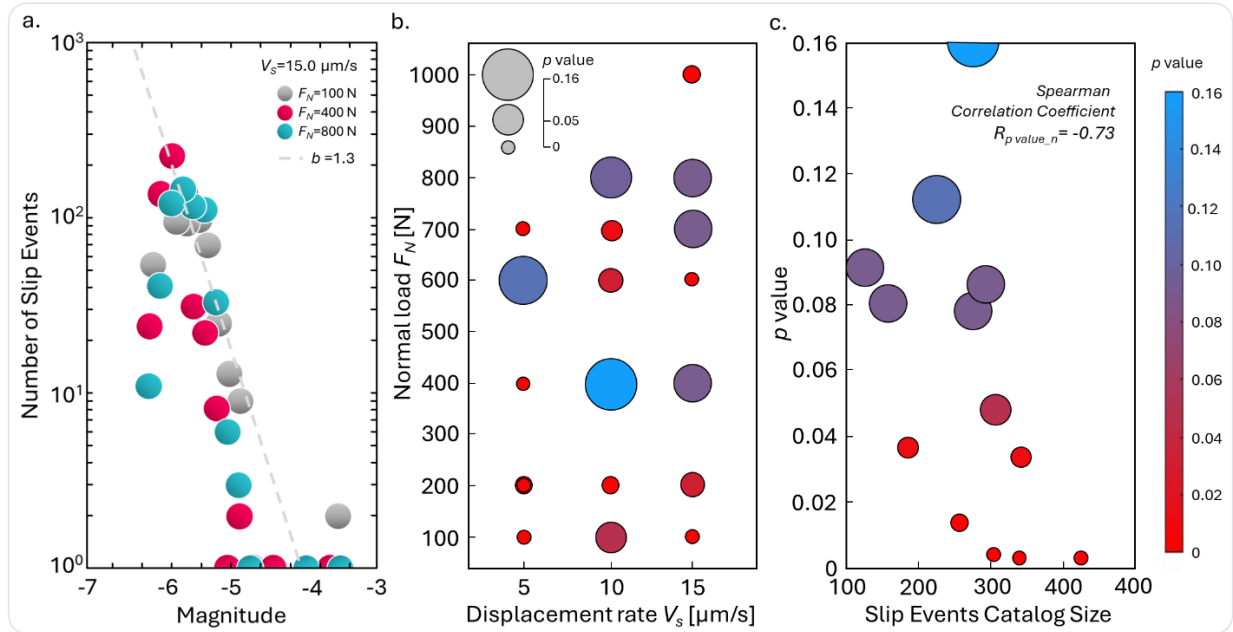
522 While mixtures of exponential distributions remain monotonic (Jewell, 1982; Heckman,  
523 1990), a mixture of an exponential and a peaked distribution, such as a normal or lognormal  
524 produces a distribution with modes or, at least, bumps. This could occur if the catalog combines  
525 background seismicity governed by exponential decay, and clustered or repeating events around  
526 a characteristic magnitude (e.g., due to local failure modes or geomechanical constraints).

527 Finally, non-stationary stress conditions and dynamic b-values may also be responsible for  
528 complex magnitude distributions. As previously noted in the manuscript, the work of Dublanchet  
529 (2020) demonstrates how stress evolution can modulate the b-value through time. In  
530 anthropogenic settings where stress evolves rapidly and non-linearly due to engineering  
531 operations, each earthquake could effectively sample a slightly different exponential distribution.  
532 When aggregated, this may lead to complex magnitude distributions that are inconsistent with a  
533 single b-value model. Furthermore, we emphasize that our statistical testing shows that even  
534 mixtures of exponential distributions with different b-values do not result in multimodal or  
535 bump-containing distributions. Thus, the observed complexity in many magnitude distributions  
536 cannot be attributed to simple mixing alone.

### 537 **4.3 Role of mixture of stable and unstable slip**

538 We would like to focus the attention on some of our observations that may be relevant for  
539 the further delving into the problem. Some earlier studies hypothesized that the different  
540 fracturing processes during the technological operations, variations in rock types, fault networks,  
541 mitigation protocols to reduce the occurrence or magnitude of AS, and the temporal evolution  
542 of human activities progress, can alter the magnitude distribution (Lasocki, 2001; Gibowicz &  
543 Lasocki, 2001; Lasocki & Orlecka-Sikora, 2008; Eaton et al., 2014; Eaton & Maghsoudi, 2015;

544 Urban et al., 2016). We analyzed the laboratory experiments of Shu et al. (2023) on the temporal  
545 evolution of the slip of asperities on a faulting interface. Even for the uniformly distributed  
546 asperities under the constant normal load and the various constant displacement rates imposed  
547 on the system, the resulted slip event magnitude distributions, although mimic the GR relation,  
548 are identified by the AD and multimodal tests as non-exponential and complex. Shu et al. (2023)  
549 proposed a novel experimental setup with a PMMA plate sliding on a customized surface with  
550 asperities modeled by numerous identical spherical PMMA beads embedded in a softer polymer  
551 base. The spatio-temporal interactions of asperities were quantified in the experiments as  
552 collective slip episodes mimicking fault ruptures including both stable and unstable slips. We  
553 examine the catalogues of slip episodes recorded for various mechanical conditions, available in  
554 Shu et al. (2023). The slip event is characterized there as a single rupture with the slow slip in the  
555 sense that the ratio of its size with respect to its duration is much lower than the Rayleigh wave  
556 speed of the material of the interface. Fig. 6 with the results of the FMD tests shows that the  
557 FMD exponentiality does not depend on the value of the normal loads and the displacement  
558 rates imposed on the system. Moreover, the  $p$  value of statistical inference depends on the  
559 number of observations in a sample – the larger sample the smaller  $p$  value, with the Spearman  
560 correlation coefficient  $R_{p\ value\_n} = -0.73$ . The results are stable after the exclusion of the large  
561 stick-slip events at the global fault scale, which reach the boundaries of the model and  
562 accordingly are limited in size. For eighteen from nineteen samples the  $p$  value of the hypotheses  
563 stating about the FMD multimodality ( $H_0^2$ ) are lower than 0.05 confirming that the magnitude  
564 distribution is complex. These results indicate that the interplay of stable and unstable slips may  
565 be responsible for the nonlinear shape and the complexity of the magnitude distribution.



566  
 567 **Figure 6. a. Frequency magnitude distribution of slip events on asperities along an analogue fault interface during**  
 568 **stick-slips at different loading rates under different normal load during the laboratory experiments performed by**  
 569 **Shu et al. (2023), b. together with the  $p$  values of the significance of the hypotheses of the FMD exponentiality**  
 570 **and c. their relation to the sample size. Statistically significant  $p$  values of Anderson-Darling test marked by the**  
 571 **circles are size and color-coded.**

572

#### 573 **4.4 Practical implications for seismic hazard assessment**

574 Our results show that relying on the GR relationship for the AS often leads to an incorrect  
 575 estimation of magnitude distribution and, consequently, to under- or overestimation of seismic  
 576 hazard and related risk. This deviation may stem from physical processes or instrumental  
 577 limitations. Regardless of its cause, the inability to apply the GR model requires adopting a non-  
 578 parametric approach for robust analysis and interpretation as no existing magnitude distribution  
 579 models are known to follow credibly non-linear and complex distributions. Therefore, the best  
 580 solution for the magnitude distribution estimation in AS is to use the kernel nonparametric  
 581 density estimator (KDE), for the first time proposed by Lasocki, et al. (2000) and Kijko, et al.

582 (2001), and further developed by Orlecka-Sikora & Lasocki (2005) and Lasocki & Orlecka-Sikora  
583 (2008). For the interval estimation of the nonparametric estimate of the magnitude distribution,  
584 the iterated bias-corrected and accelerated method (IBCa method) has been developed (Orlecka-  
585 Sikora, 2004; 2008). The present version of this estimator, implemented in applications accessible  
586 on the EPISODES platform, utilizes Gaussian adaptive kernels (see: Supplementary Note 4), but  
587 works on its improvements are on the way.

588 Fig. 7 presents the results of the estimation of complex magnitude distribution by means of  
589 KDE and the maximum likelihood estimator (MLE) with the exponential model, and the estimates  
590 of related basic seismic hazard parameters:  $R(M, D)$  - the exceedance probability of magnitude  
591  $M$  in a time  $D$ , defined as:

$$592 \quad R(M, D) = 1 - \exp [-\lambda \cdot D \cdot (1 - CDF(M))], \quad (2)$$

593  
594 where  $\lambda$  is the mean activity rate, and  $T(M)$  - the mean return period defined as the reciprocal  
595 of the rate of occurrence of earthquakes of magnitude  $M$  or greater (e.g. Lomnitz, 1974; Baker,  
596 2008):

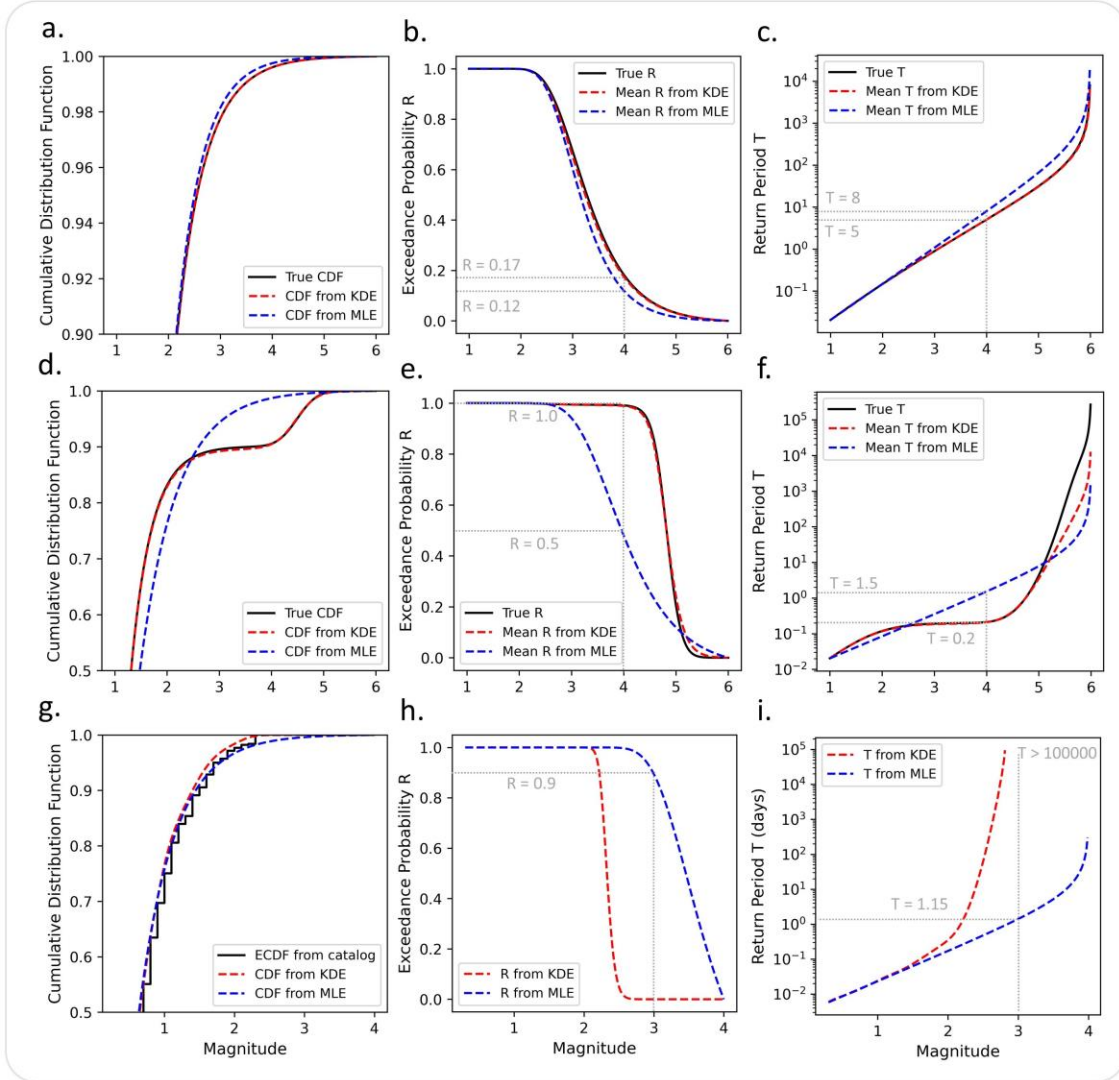
$$597 \quad T(M) = \{\lambda \cdot (1 - CDF(M))\}^{-1}. \quad (3)$$

598 The  $CDF(M)$ ,  $R(M, D)$ , and  $T(M)$  are estimated from synthetic datasets which include a  
599 mixed sample from two exponential distributions with different  $b$  values and a mixed sample  
600 from the exponential and normal distributions accounting for the characteristic-earthquake  
601 hypothesis (Igonin et al., 2018). They are also estimated using the empirical CDF (ECDF) from a  
602 real AS dataset, associated with the geothermal energy production – the Soultz-Sous-Forets 2004  
603 episode in EPISODES Platform (EOST & GEIE EMC, 2018). For both synthetic datasets the KDE

604 estimates are much closer to the actual *CDF*, *R*, and *T*, than MLE estimates (Fig. 7). E.g., for the  
605 dataset from model 1, the actual exceedance probability *R* for the magnitude  $M = 4$  in  $D = 1$   
606 time units is 0.17, whereas the MLE estimate is equal 0.12. This divergence is also reflected in *T*  
607 estimate, i.e. for the magnitude  $M = 4$  we have  $T = 5$  but the parametric estimate is 8 time units  
608 (Fig. 7a–c). On the contrary, the KDE estimates are practically the same as the true values of *CDF*,  
609 *R*, and *T* functions.

610 In the case of model 2, both the actual value and the KDE estimate of the exceedance  
611 probability, *R* for the magnitude  $M = 4$  in  $D = 1$  time units is close to 1.0, whereas MLE  
612 significantly underestimates *R*, being equal to 0.47. The real value of the mean return period  
613 *T* for  $M = 4$  is 0.2 time units, the nonparametric estimate provides exactly the same value, but  
614 the parametric estimate is 1.5 time units.

615 We observe also the significant differences in the parametric and nonparametric estimates  
616 of *R* and *T* for the real dataset. For the  $M = 3$  we receive the parametric estimate of *R* close to  
617 0 while for the nonparametric estimate it is approximately 0.90. The mean return period, *T*  
618 estimated by MLE is 0.3 days but when we apply the nonparametric approach *T* is equal to more  
619 than 100000 days. The above examples show that when the FMD is complex, the classic, GR  
620 model-based approach results in systematic very significant estimation errors. AS is controlled by  
621 a time changeable production process therefore assuming the GR relation-born magnitude  
622 distribution for AS is in many cases not valid. A short-term, detailed analysis of the seismic  
623 hazards for AS must assess time-variations of probabilistic distributions of source parameters.



624  
625 **Figure 7. Probability Density Function of magnitudes  $CDF(M)$ , the exceedance probability in  $D$  time  $R(M, D =$   
626 **1) and the mean return period  $T(M)$  for a. - c. the synthetic 400-elements dataset drawn from the mixture of the**  
627 **two exponential distributions with the exponents of  $b = 0.7$  and  $b = 1.1$  in equal proportions (model 1); d. - f. the**  
628 **synthetic 400-elements dataset drawn from the mixture of the exponential and normal distributions with the**  
629 **parameters: the exponent  $b = 1.1$ , the expected value  $\mu = 4.5$  and the standard deviation  $\sigma = 0.3$ , in equal**  
630 **proportions (model 2); g. - i. the real dataset: the SOULTZ-SOUS-FORETS 2004 episode in EPISODES Platform,**  
631 **containing 3266 earthquakes between September 13 and 16 2004, with a  $M_c = 0.3$ . In both models, the  $CDF$ ,  $R$ ,**  
632 **and  $T$  are the average over 100 000 simulations. The GR Maximum Likelihood Estimator found an average  $b$  value**  
633 **of 0.86 for the model 1, 0.62 for the model 2 and 0.55 for the real dataset.****

634

## 635 5. Summary and Conclusions

636 We analyzed 63 FMDs resulting from 18 AS episodes associated with various technological  
637 activities and found that nearly half (47.6%) does not accord with the exponential distribution,  
638 hence does not follow the Gutenberg - Richter relation. Among these, 16 exhibit complex  
639 features such as multiple bumps or modes. Similar deviations have been reported in previous  
640 studies and in natural seismicity, often attributed to the mixing of seismic zones or clusters with  
641 different b-values. Our simulations show that such mixing leads to testable deviations from  
642 exponentiality only when sample sizes are large or the particular b-values are significantly  
643 different. The analysis of b values in the selected FMDs suggests that the mixing cannot explain  
644 the observed deviations. Moreover, the mixtures of exponential distributions which are  
645 monotonic, hence cannot explain the observed complex features in the mentioned sixteen cases.

646 Our study shows that in many cases there are complex magnitude distributions and this  
647 complexity reflects the dynamic industrial processes and in some case complex geological  
648 settings. In such cases the use of classical GR model can impact seismic hazard assessment. The  
649 comparative analysis with real and synthetic datasets shows that using a kernel nonparametric  
650 density estimator (KDE) outperforms traditional MLE in capturing the true characteristics of  
651 complex AS magnitude distributions. KDE should therefore be considered a standard tool for  
652 estimating seismic hazard parameters. Additionally, we highlight the potential of an adaptive  
653 kernel method that accounts for data sparsity as a more advanced alternative (Orlecka-Sikora  
654 and Lasocki, 2005).

655 Future work should aim to bridge the gap between statistical observations and the underlying  
656 physical processes driving induced seismicity. The complexity observed in FMDs, including

657 deviations from exponentiality and multimodal patterns, suggests the involvement of distinct  
658 rupture processes or evolving fault conditions that merit further investigation. The assumption  
659 of an exponential frequency–magnitude distribution is fundamental for applying the Gutenberg–  
660 Richter model and interpreting b-values. Kijko et al., (2001) showed that when this assumption  
661 is violated, applying the G–R model can lead to significant underestimation of seismic hazard,  
662 and they advocated for nonparametric approaches that do not rely on the exponentiality of the  
663 FMD. Alternative approaches have also shown promise: for example, a particle filter approach  
664 (Iwata and Nanjo, 2024) effectively captures the temporal variability of b-values, while a moving  
665 window combined with a kernel of the arithmetic mean can account for spatial variability (Pardo-  
666 Igúzquiza and Dowd, 2024). These approaches are particularly well-suited for analyzing induced  
667 seismicity, where both temporal and spatial variations are intrinsic features. Incorporating an  
668 improved non-parametric approach and machine-learning approaches may better capture  
669 evolving distributional characteristics without strict parametric assumptions. Ultimately,  
670 embedding these tools into real-time monitoring systems could support adaptive strategies  
671 aimed at minimizing seismic hazard.

672

673 **Data and Resources**

674 All data used in the analysis are available on the EPISODES platform of the Thematic Core Service  
675 Anthropogenic Hazards of the European Plate Observing System ([Orlecka-Sikora et al., 2020](#)):  
676 <https://episodesplatform.eu/?lang=en>. This data is licensed under the Creative Commons  
677 Attribution 4.0 International License, CC:BY. All data needed to evaluate the conclusions in the  
678 paper are presented in the main text of the paper and the Supplementary Notes. Figures were  
679 made by Matlab software, License Number: 40837060 and Statistica 13 software, Licence  
680 Number: ANS009K287811A136-4 and by Python's Matplotlib library (Hunter, 2007).

681

682 **Code availability**

683 The used codes in the paper are available on the EPISODES platform of the Thematic Core Service  
684 Anthropogenic Hazards of the European Plate Observing System ([Orlecka-Sikora et al., 2020](#)):  
685 <https://episodesplatform.eu/?lang=en>.

686

687 **Acknowledgements**

688 We would like to thank Olivier Lengline and Weiwei Shu for the access to the experimental data  
689 from Shu et al. (2023) (<https://doi.org/10.25577/2023-SHU-JGR>). Administrative support, article  
690 publishing charges, travel, and writing assistance were provided by Institute of Geophysics Polish  
691 Academy of Sciences.

692

693 **References**

- 694 Adushkin, V. V. (2016). Tectonic earthquakes of anthropogenic origin, *Izvestiya, Physics of the*  
695 *Solid Earth* **52**, no. 2, 173–194, doi: 10.1134/S1069351316020014.
- 696 AKI, K. (1965). Maximum likelihood estimate of b in the formula  $\log N=a-bM$  and its confidence  
697 limits, *Bull. Earthquake Res. Inst., Tokyo Univ.* **43**, 237–239.
- 698 Amorese, D. (2007). Applying a Change-Point Detection Method on Frequency-Magnitude  
699 Distributions. *Bulletin of the Seismological Society of America*, *97*(5), 1742–1749.  
700 <https://doi.org/10.1785/0120060181>
- 701 Anderson, T. W., and D. A. Darling (1954). A Test of Goodness of Fit, *J Am Stat Assoc* **49**, no. 268,  
702 765, doi: 10.2307/2281537.
- 703 Baisch, S., E. Rothert, H. Stang, R. Vörös, C. Koch, and A. McMahon (2015). Continued Geothermal  
704 Reservoir Stimulation Experiments in the Cooper Basin (Australia), *Bulletin of the*  
705 *Seismological Society of America* **105**, no. 1, 198–209, doi: 10.1785/0120140208.
- 706 Baisch, S., R. Voros, R. Weidler, and D. Wyborn (2009). Investigation of Fault Mechanisms during  
707 Geothermal Reservoir Stimulation Experiments in the Cooper Basin, Australia, *Bulletin of the*  
708 *Seismological Society of America* **99**, no. 1, 148–158, doi: 10.1785/0120080055.
- 709 Baisch, S., R. Weidler, R. Vörös, D. Wyborn, and L. de Graaf (2006). Induced seismicity during the  
710 stimulation of a geothermal HFR reservoir in the Cooper Basin, Australia, *Bulletin of the*  
711 *Seismological Society of America* **96**, no. 6, 2242–2256, doi: 10.1785/0120050255.
- 712 Baker, J.W. (2008). An introduction to probabilistic seismic hazard analysis (PSHA). Version 1.3.  
713 pp.

714 72.[http://www.stanford.edu/~bakerjw/Publications/Baker\\_\(2008\)\\_Intro\\_to\\_PSHA\\_v1\\_3.p](http://www.stanford.edu/~bakerjw/Publications/Baker_(2008)_Intro_to_PSHA_v1_3.pdf)  
715 [df](http://www.stanford.edu/~bakerjw/Publications/Baker_(2008)_Intro_to_PSHA_v1_3.pdf). Accessed 01 Oct 2008.

716 Bender, B. (1983). Maximum likelihood estimation of  $b$  values for magnitude grouped data,  
717 *Bulletin of the Seismological Society of America* **73**, no. 3, 831–851, doi:  
718 10.1785/BSSA0730030831.

719 Bethmann, F., Deichmann, N., & Mai, P. M. (2011). Scaling Relations of Local Magnitude versus  
720 Moment Magnitude for Sequences of Similar Earthquakes in Switzerland. *Bulletin of the*  
721 *Seismological Society of America*, *101*(2), 515–534. <https://doi.org/10.1785/0120100179>

722 Cox, D. R. (1966). Notes on the analysis of mixed frequency distributions, *British Journal of*  
723 *Mathematical and Statistical Psychology* **19**, no. 1, 39–47, doi: 10.1111/j.2044-  
724 8317.1966.tb00353.x.

725 Davies, R., G. Foulger, A. Bindley, and P. Styles (2013). Induced seismicity and hydraulic fracturing  
726 for the recovery of hydrocarbons, *Mar Pet Geol* **45**, 171–185, doi:  
727 10.1016/j.marpetgeo.2013.03.016.

728 Deichmann, N. (2017). Theoretical Basis for the Observed Break in  $M_L/M_w$  Scaling between Small  
729 and Large Earthquakes. *Bulletin of the Seismological Society of America*, *107*(2), 505–520.  
730 <https://doi.org/10.1785/0120160318>

731 Dublanchet, P. (2020). Stress-Dependent  $b$  Value Variations in a Heterogeneous Rate-and-State  
732 Fault Model, *Geophys Res Lett* **47**, no. 13, doi: 10.1029/2020GL087434.

733 Eaton, D. W., J. Davidsen, P. K. Pedersen, and N. Boroumand (2014). Breakdown of the  
734 Gutenberg-Richter relation for microearthquakes induced by hydraulic fracturing: Influence

735 of stratabound fractures, *Geophys Prospect* **62**, no. 4, 806–818, doi: 10.1111/1365-  
736 2478.12128.

737 Eaton, D. W., and S. Maghsoudi (2015). 2b... or not 2b? Interpreting magnitude distributions from  
738 microseismic catalogs, *First Break* **33**, no. 10, doi: 10.3997/1365-2397.33.10.83159.

739 Edwards, B., & Douglas, J. (2014). Magnitude scaling of induced earthquakes. *Geothermics*, *52*,  
740 132–139. <https://doi.org/10.1016/j.geothermics.2013.09.012>

741 Efron, B., & Tibshirani, R. J., *An Introduction to the Bootstrap*. New York: Chapman and Hall  
742 (1998).

743 Feustel, A.J. (1997) Temporal-spatial b-values and observed relationships to structurally  
744 controlled ground falls in an open-stope mine, Proc 4th Int Symp on Rockburst and Seismicity  
745 in Mines, Gibowicz, S.J. and Lasocki, S. (eds), Balkema, Netherlands, pp. 191–195.

746 Foulger, G. R., M. P. Wilson, J. G. Gluyas, B. R. Julian, and R. J. Davies (2018). Global review of  
747 human-induced earthquakes, *Earth Sci Rev* **178**, 438–514, doi:  
748 10.1016/j.earscirev.2017.07.008.

749 Geffers, G.-M., I. G. Main, and M. Naylor (2022). Biases in estimating *b* -values from small  
750 earthquake catalogues: how high are high *b* -values?, *Geophys J Int* **229**, no. 3, 1840–1855,  
751 doi: 10.1093/gji/ggac028.

752 Gibowicz, S. J., and Andrzej. Kijko (1994). An introduction to mining seismology, 399.

753 Gibowicz, S. J., and S. Lasocki (2001). Seismicity induced by mining: Ten years later, *Advances in*  
754 *Geophysics* **44**, no. C, 39–181, doi: 10.1016/S0065-2687(00)80007-2.

755 Goertz-Allmann, B. P., Edwards, B., Bethmann, F., Deichmann, N., Clinton, J., Fah, D., & Giardini,  
756 D. (2011). A New Empirical Magnitude Scaling Relation for Switzerland.

757 Gong W, Chen H, Gao Y, Li Q and Sun Y (2024), A test on methods for Mc estimation and spatial-  
758 temporal distribution of b-value in the eastern Tibetan Plateau. *Front. Earth Sci.* 12:1335938.  
759 doi: 10.3389/feart.2024.1335938

760 Grigoli, F., S. Cesca, E. Priolo, A. P. Rinaldi, J. F. Clinton, T. A. Stabile, B. Dost, M. G. Fernandez, S.  
761 Wiemer, and T. Dahm (2017). Current challenges in monitoring, discrimination, and  
762 management of induced seismicity related to underground industrial activities: A European  
763 perspective, *Reviews of Geophysics* **55**, no. 2, 310–340, doi: 10.1002/2016RG000542.

764 Gutenberg, B., and C. F. Richter (1944). Frequency of earthquakes in California, *Bulletin of the*  
765 *Seismological Society of America* **34**, no. 4, 185–188, doi: 10.1785/BSSA0340040185.

766 Heckman, J. J., R. Robb, and J. R. Walker (1990). Testing the Mixture of Exponentials Hypothesis  
767 and Estimating the Mixing Distribution by the Methods of Moments, *J Am Stat Assoc* **85**, no.  
768 410, 582, doi: 10.2307/2289802.

769 Herrmann, M., and W. Marzocchi (2021). Inconsistencies and Lurking Pitfalls in the Magnitude–  
770 Frequency Distribution of High-Resolution Earthquake Catalogs, *Seismological Research*  
771 *Letters* **92**, no. 2A, 909–922, doi: 10.1785/0220200337.

772 Herrmann, M., E. Piegari, and W. Marzocchi (2022). Revealing the spatiotemporal complexity of  
773 the magnitude distribution and b-value during an earthquake sequence, *Nat Commun* **13**,  
774 no. 1, 1–10, doi: 10.1038/s41467-022-32755-6.

775 Huang, Y., and G. C. Beroza (2015). Temporal variation in the magnitude-frequency distribution  
776 during the Guy-Greenbrier earthquake sequence, *Geophys Res Lett* **42**, no. 16, 6639–6646,  
777 doi: 10.1002/2015GL065170.

778 Hunter, J. D. (2007). Matplotlib: A 2D Graphics Environment, *Comput Sci Eng* **9**, no. 3, 90–95, doi:  
779 10.1109/MCSE.2007.55.

780 Igonin, N., M. Zecevic, and D. W. Eaton (2018). Bilinear Magnitude-Frequency Distributions and  
781 Characteristic Earthquakes During Hydraulic Fracturing, *Geophys Res Lett* **45**, no. 23, doi:  
782 10.1029/2018GL079746.

783 Iwata, D., and K. Z. Nanjo (2024). Adaptive estimation of the Gutenberg–Richter b value using a  
784 state space model and particle filtering, *Sci Rep* **14**, no. 1, 4630, doi: 10.1038/s41598-024-  
785 54576-x.

786 IS EPOS (2020), Episode: COOPER BASIN, [https://episodesplatform.eu/#episode:COOPER\\_BASIN](https://episodesplatform.eu/#episode:COOPER_BASIN),  
787 doi:10.25171/InstGeoph\_PAS\_ISEPOS-2020-001

788 Jewell, N. P. (1982). Mixtures of Exponential Distributions, *The Annals of Statistics* **10**, no. 2, doi:  
789 10.1214/aos/1176345789.

790 Johnston, J.C. and H.H. Einstein A survey of mining associated rockbursts. In *Rockbursts and*  
791 *Seismicity in Mines: Dynamic rock mass response to mining* (Fairhurst, C, ed.) (A.A Balkema,  
792 Rotterdam 1990), pp. 121-128.

793 Kijko, A., B. Drzęźła, B., and T. Stankiwicz (1987) Bimodal character of extreme seismic events in  
794 Polish mines. *Acta Geophys. Polonica* **35**, 157-166.

795 Kijko, A., S. Lasocki, and G. Graham (2001). Non-parametric Seismic Hazard in Mines, *Pure Appl*  
796 *Geophys* **158**, no. 9, 1655–1675, doi: 10.1007/PL00001238.

797 Kinscher, J., S. Cesca, P. Bernard, I. Contrucci, A. Mangeney, J. P. Piguët, and P. Bigarré (2016).  
798 Resolving source mechanisms of microseismic swarms induced by solution mining,  
799 *Geophys J Int* **206**, no. 1, 696–715, doi: 10.1093/gji/ggw163.

800 Krushelnitskii, K. V., P. N. Shebalin, I. A. Vorobieva, O. V. Selyutskaya, and A. O. Antipova (2024).  
801 The Limits of Applicability of the Gutenberg–Richter Law in the Problems of Seismic Hazard  
802 and Risk Assessment, *IZV-PHYS SOLID EART* **60**, no. 5, 823–835, doi:  
803 10.1134/S1069351324700757.

804 Lasocki, S., Kijko, A., & Graham, G. Model-free seismic hazard estimation, In H. Gokcekus (Ed.),  
805 Proc. Int. Conf. Earthquake Hazard and Risk in the Mediterranean Region, EHRMR'99  
806 (Educational Foundation of Near East University, Lefkosia, T. R. N. Cyprus ) (pp. 503–508)  
807 (2000).

808 Lasocki, S., Quantitative evidences of complexity of magnitude distribution in mining-induced  
809 seismicity: Implications for hazard evaluation, In Rockbursts and Seismicity in Mines:  
810 Dynamic rock mass response to mining (vanAswegen,G.,Durrheim, R.J.,Ortlepp, W.D. eds.)  
811 (SAIMM S27, Johannesburg, 2001), pp. 543-550.

812 Lasocki, S., and B. Orlecka-Sikora (2008). Seismic hazard assessment under complex source size  
813 distribution of mining-induced seismicity, *Tectonophysics* **456**, no. 1–2, 28–37, doi:  
814 10.1016/j.tecto.2006.08.013.

815 Lasocki, S., and Orlecka-Sikora, B, “Anthropogenic Seismicity Related to Exploitation of  
816 Georesources” in Encyclopedia of Solid Earth Geophysics. Encyclopedia of Earth Sciences  
817 Series, H.K. Gupta, Ed. (Springer, Cham, 2020).

818 Lasocki, S., B. Orlecka-Sikora, J. Kocot, K. Chodzińska, and A. Leśnodorska (2022). EPOS Thematic  
819 Core Service Anthropogenic Hazards in the operational phase, *Annals of Geophysics* **65**, no.  
820 3, DM321, doi: 10.4401/ag-8743.

821 Lasocki, S., and E. E. Papadimitriou (2006). Magnitude distribution complexity revealed in  
822 seismicity from Greece, *J Geophys Res Solid Earth* **111**, no. 11, 1–18, doi:  
823 10.1029/2005JB003794.

824 Leptokaropoulos, K. (2020). Magnitude distribution complexity and variation at the Geysers  
825 geothermal field, *Geophys J Int* **222**, no. 2, 893–906, doi: 10.1093/gji/ggaa208.

826 Leptokaropoulos, K. M., V. G. Karakostas, E. E. Papadimitriou, A. K. Adamaki, O. Tan, and S. Inan  
827 (2013). A homogeneous earthquake catalog for western Turkey and magnitude of  
828 completeness determination, *Bulletin of the Seismological Society of America* **103**, no. 5,  
829 2739–2751, doi: 10.1785/0120120174.

830 Lilliefors, H. W. (1967). On the Kolmogorov-Smirnov Test for Normality with Mean and Variance  
831 Unknown, *J Am Stat Assoc* **62**, no. 318, 399, doi: 10.2307/2283970.

832 Lizurek, G., J. Wiszniowski, N. Van Giang, B. Plesiewicz, and D. Q. Van (2017). Clustering and Stress  
833 Inversion in the Song Tranh 2 Reservoir, Vietnam, *Bulletin of the Seismological Society of*  
834 *America* **107**, no. 6, 2636–2648, doi: 10.1785/0120170042.

835 Lizurek, G., K. Leptokaropoulos, J. Wiszniowski, N. Van. Giang, I. Nowaczyńska, B. Plesiewicz, D.  
836 Q. Van, and A. Tymińska (2021). Seasonal trends and relation to water level of reservoir-  
837 triggered seismicity in Song Tranh 2 reservoir, Vietnam, *Tectonophysics* **820**, 229121, doi:  
838 10.1016/j.tecto.2021.229121.

839 Lomnitz, C., Global tectonics and earthquake risk. Amsterdam: Elsevier Sc. Publ. Co (1974).

840 Maghsoudi, S., S. Hainzl, S. Cesca, T. Dahm, and D. Kaiser (2013). Identification and  
841 characterization of growing large-scale en-echelon fractures in a salt mine, *Geophys J Int*  
842 **196**, no. 2, 1092–1105, doi: 10.1093/gji/ggt443.

843 Mallika, K., H. Gupta, D. Shashidhar, N. P. Rao, A. Yadav, S. Rohilla, H. V. S. Satyanarayana, and D.  
844 Srinagesh (2013). Temporal variation of b value associated with  $M \sim 4$  earthquakes in the  
845 reservoir-triggered seismic environment of the Koyna–Warna region, Western India, *J*  
846 *Seismol* **17**, no. 1, 189–195, doi: 10.1007/s10950-012-9318-3.

847 Marzocchi, W., and Sandri, L. (2009). A review and new insights on the estimation of the b-  
848 value and its uncertainty, *Annals of Geophysics* **46**, no. 6, doi: 10.4401/ag-3472.

849 Marzocchi, W., I. Spassiani, A. Stallone, and M. Taroni (2020). Erratum to: How to be fooled  
850 searching for significant variations of the b-value, *Geophys J Int* **221**, no. 1, 351–351, doi:  
851 10.1093/gji/ggaa061.

852 McGarr A, Simpson D, Seeber L (2002) Case histories of induced and triggered seismicity. In: Lee  
853 WHK, Kanamori H, Jennings PC, Kisslinger C (eds) International handbook of earthquake and  
854 engineering seismology, part A. Academic Press, London, pp 647–66

855 Olszewska, D., S. Lasocki, and K. Leptokaropoulos (2017). Non-stationarity and internal  
856 correlations of the occurrence process of mining-induced seismic events, *Acta Geophysica*  
857 **65**, no. 3, 507–515, doi: 10.1007/s11600-017-0024-y.

858 Orlecka-Sikora, B. (2004). Bootstrap and jackknife resampling for improving in the nonparametric  
859 seismic hazard estimation, In Y.T. Chen, G.F. Panza, Z.L. Wu. (Eds.), The IUGG 2003  
860 Proceedings Volume “Earthquake. Hazard, Risk, and Strong Ground Motion” (pp. 81–92).  
861 Seismological Press.

862 Orlecka-Sikora, B., Lasocki, S. Nonparametric characterization of mining induced seismic sources,  
863 In Y. Potvin, & M. Hudyma (Eds.), The Sixth International Symposium on Rockbursts and  
864 Seismicity in Mines “Controlling Seismic Risk” Proceedings (pp. 555–560). Perth: ACG (2005).

865 Orlecka-Sikora, B. (2008). Resampling methods for evaluating the uncertainty of the  
866 nonparametric magnitude distribution estimation in the Probabilistic Seismic Hazard  
867 Analysis, *Tectonophysics* **456**, no. 1–2, 38–51, doi: 10.1016/j.tecto.2007.01.026.

868 Orlecka-Sikora, B., S. Lasocki, J. Kocot, T. Szepieniec, J. R. Grasso, A. Garcia-Aristizabal, M.  
869 Schaming, P. Urban, G. Jones, I. Stimpson, *et al.* (2020). An open data infrastructure for the  
870 study of anthropogenic hazards linked to georesource exploitation, *Sci Data* **7**, no. 1, 1–16,  
871 doi: 10.1038/s41597-020-0429-3.

872 Orlecka-Sikora, B., Ł. Rudziński, M. Staszek, G. Lizurek, and K. Mizerski (2023). Seismic swarms as  
873 intermittent quasi-static ruptures driven by pore pressure variations due to the water  
874 reservoir impoundment, *Tectonophysics* **863**, 230005, doi: 10.1016/j.tecto.2023.230005.

875 Pardo-Igúzquiza, E., and P. A. Dowd (2024). Inference of the Gutenberg-Richter b-value: New  
876 insights and results, *Tectonophysics* **890**, 230486, doi: 10.1016/j.tecto.2024.230486.

877 Pelz, M.-T., M. Schartau, C. J. Somes, V. Lampe, and T. Slawig (2023). A diffusion-based kernel  
878 density estimator (diffKDE, version 1) with optimal bandwidth approximation for the analysis  
879 of data in geoscience and ecological research, *Geosci Model Dev* **16**, no. 22, 6609–6634, doi:  
880 10.5194/gmd-16-6609-2023.

881 Plotnikova, L. M., B. S. Nurtaev, J. R. Grasso, L. M. Matasova, and R. Bossu (1996). The character  
882 and extent of seismic deformation in the focal zone of gazli earthquakes of 1976 and  
883 1984, *M&gt;7.0, Pure and Applied Geophysics PAGEOPH* **147**, no. 2, 377–387, doi:  
884 10.1007/BF00877490.

885 Rutledge, J. T. (2004). Faulting Induced by Forced Fluid Injection and Fluid Flow Forced by  
886 Faulting: An Interpretation of Hydraulic-Fracture Microseismicity, Carthage Cotton Valley

887 Gas Field, Texas, *Bulletin of the Seismological Society of America* **94**, no. 5, 1817–1830, doi:  
888 10.1785/012003257.

889 Shebalin, P. N., S. V. Baranov, I. A. Vorobieva, E. M. Grekov, K. V. Krushelnitskii, A. A. Skorkina,  
890 and O. V. Selyutskaya (2024). Seismicity Modeling in Tasks of Seismic Hazard Assessment,  
891 *Dokl. Earth Sci* **515**, no 1, 514–525, doi: 10.1134/S1028334X23603115.

892 Shu, W., O. Lengliné, and J. Schmittbuhl (2023). Collective Behavior of Asperities Before Large  
893 Stick-Slip Events, *J Geophys Res Solid Earth* **128**, no. 9, doi: 10.1029/2023JB026696.

894 Silverman, B. W., Density Estimation for Statistics and Data Analysis, (Chapman Hall, London  
895 1986).

896 Slakter, M. J. (1965). A Comparison of the Pearson Chi-Square and Kolmogorov Goodness-of-Fit  
897 Tests with Respect to Validity, *J Am Stat Assoc* **60**, no. 311, 854, doi: 10.2307/2283251.

898 Stephens, M. A. (1974). EDF Statistics for Goodness of Fit and Some Comparisons, *J Am Stat Assoc*  
899 **69**, no. 347, 730, doi: 10.2307/2286009.

900 Styles P., Gasparini P., Huenges E., Scandone P., Lasocki S., Terlizzese F. - International  
901 Commission On Hydrocarbon Exploration And Seismicity In The Emilia Region (ICHESE)  
902 (2014) Report on the hydrocarbon exploration and seismicity in Emilia Region,  
903 <http://unmig.sviluppoeconomico.gov.it/unmig/agenda/dettaglionotizia.asp?id=175>)

904 Subbaramu, K.R., Rao, B.S.S., Krishnamurthy, R. and Srinivasan, C. (1989) Seismic investigations  
905 of rockbursts in the Kolar Gold Fields, Proc. 4th Conf. Acoustic Emission/Microseismic  
906 Activity in Geologic Structures and Materials, Penn State University, H.R. Hardy, Jr. (editor),  
907 Clausthal, Trans Tech Publications, pp. 265–274.

908 Trifu, C-I., Urbancic, T.I. and Young, R.P. (1993) Non-similar frequency-magnitude distribution for  
909  $m < 1$  seismicity, *Geophys Res Lett.* **20**, 427–430

910 Urban, P., S. Lasocki, P. Blascheck, A. F. do Nascimento, N. Van Giang, and G. Kwiatek (2016).  
911 Violations of Gutenberg–Richter Relation in Anthropogenic Seismicity, *Pure Appl Geophys*  
912 **173**, no. 5, 1517–1537, doi: 10.1007/s00024-015-1188-5.

913 Valoroso, L., L. Improta, L. Chiaraluce, R. Di Stefano, L. Ferranti, A. Govoni, and C. Chiarabba  
914 (2009). Active faults and induced seismicity in the Val d’Agri area (Southern Apennines, Italy),  
915 *Geophys J Int* **178**, no. 1, 488–502, doi: 10.1111/j.1365-246X.2009.04166.x.

916 Vilarrasa, V., S. De Simone, J. Carrera, and A. Villaseñor (2021). Unraveling the Causes of the  
917 Seismicity Induced by Underground Gas Storage at Castor, Spain, *Geophys Res Lett* **48**, no.  
918 7, doi: 10.1029/2020GL092038.

919 Węglarczyk, S., and S. Lasocki (2009). Studies of short and long memory in mining-induced seismic  
920 processes, *Acta Geophysica* **57**, no. 3, 696–715, doi: 10.2478/s11600-009-0021-x.

921 Wesnousky, S. G. (1994). The Gutenberg-Richter or characteristic earthquake distribution, which  
922 is it? *Bull. Seism. Soc. Am.* **84**, 1940-1959.

923 Wiemer, S., and M. Wyss (2000). Minimum magnitude of completeness in earthquake catalogs:  
924 Examples from Alaska, the Western United States, and Japan, *Bulletin of the Seismological*  
925 *Society of America* **90**, no. 4, 859–869, doi: 10.1785/0119990114.

926

927 **Statements & Declarations**

928

929 **Author contributions**

930 Author Contributions: Conceptualization: BOS, SL, AK; Data curation: AK; Funding acquisition:

931 BOS; Investigation: AK, BOS, SL, FT; Software: SL, AK, FT; Supervision and validation: BOS, SL;

932 Visualization: AK, FT, BOS; Writing – original draft: AK, BOS, FT; Writing – review & editing: BOS,

933 SL.

934

935 **Competing interests**

936 The authors declare that they have no competing interests.

937

938 **Funding**

939 The work presented in this paper was supported by the project DT-Geo funded by Horizon Europe

940 under the grant agreement No 101058129.

941

942 **Appendix A – Magnitude of completeness methods comparison**

943 **Table A1** The results of the five examined methods for the magnitude of completeness ( $M_c$ ) calculations of the  
 944 selected catalogs. The highest calculated  $M_c$  for each catalog is colored by green and the second highest by yellow.  
 945 The method of mGFT, noted by a star (\*), is selected for all catalogs because it provides almost consistently the  
 946 highest or second highest estimation. Outlier values are filled with a dark blue and not considered.

Catalog	M <sub>c</sub> method				
	MaxCurv	GFT10	GFT5	mGFT *	MBASS
Cooper 2005 – North cluster	-0.4	-0.5	1.2	-0.2	-0.2
Cooper 2005 – South cluster	-0.5	-0.5	0.6	-0.3	-0.3
Cooper 2012 – 1st injection	-1	-1.1	-0.9	-0.8	-1
Cooper 2012 – 2nd Injection	-1	-1.1	-0.3	0	-0.6
Soultz-Sous-Forets 1993	-1.7	-1.8	-1.7	-1.6	-1.5
Soultz-Sous-Forets 2004	-1.2	-1.3	0.4	0.3	-1.1
Soultz-Sous-Forets 2005	-0.7	-1	0.7	-0.4	-0.7
St. Gallen	-0.6	-0.6		-0.6	-0.6
The Geysers - Prati 9 and 29	1.4	1.6	2	2	
Carbfix – Center (Blue)	0.9	0.8	0.9	0.8	0.9
Carbfix – Center (magenta)	0.9	0.8		0.8	
Carbfix – East (green)	1	1.1		1	0.9
Carbfix – East (red)	0.9	0.9		0.9	0.9
Carbfix – North (yellow)	1.1	1.2		1	1.1
Carbfix – North (cyan)	1.2			1	
Cotton Valley	-2.1	-2.1		-2	-2.1
Groningen 1992-2011	1.2	1.1	1.2	1.2	1.4
Groningen 2011-2015	0.9	0.8		0.9	0.9
Groningen 2015-2022	0.6	0.5		0.6	
LACQ 1969-1996	2.4	2.2		2.2	
LACQ 1996-2009	1.8	1.7	3.3	1.8	1.8
Gazli 1991	0.5	0.7	0.8	0.8	
Starfish 1st cycle – Period 1	-4.8	-4.4	-3.6	-4.2	-4.8
Starfish 1st cycle – Period 2	-4.4	-4.4	-4	-4.3	-4.3
Starfish 2nd cycle	-5.1	-5	-4.6	-4.6	-4.8
Starfish 3rd cycle	-5.1	-5.1	-4.8	-4.8	-5
Starfish 4th cycle – Period 1	-5.2	-5.1	-4.9	-4.7	-5
Starfish 4th cycle – Period 2	-5.1	-5	-4.7	-4.6	-4.8
Gisos – CERVILLE 2008	-1.2	-1.3	-0.9	-0.7	-1.2
Gisos – CERVILLE 2009	-1.1	-1.2	-0.9	-0.7	-1.1
Pyhasalmi – NE cluster	-1.4	-1.2		-0.9	-1.1
Pyhasalmi – NW cluster	-1.1	-1.1		-1	-1.1

Catalog	M <sub>c</sub> method				
	MaxCurv	GFT10	GFT5	mGFT *	MBASS
LGCD – Cluster 1	2	2	2.3	2.1	2
LGCD – Cluster 2	2	1.9		1.9	2
LGCD – Cluster 3	1.8	1.8	2	1.9	2
LGCD – Cluster 4	1.9	1.8		1.8	1.9
LGCD – Cluster 5	1.5	1.4	1.7	1.5	
LGCD – Cluster 6	1.7	1.6	1.7	1.7	1.7
LGCD – Cluster 7	1.9	1.7		1.7	1.9
LGCD – Cluster 8	1.7	1.6	3.3	1.7	1.7
LGCD – Cluster 9	1.8	1.8	2.1	1.9	1.8
LGCD – Cluster 10	1.8	1.6	1.8	1.8	1.8
LGCD – Cluster 11	2	1.7		1.9	
LGCD – Cluster 12	1.8	1.8	2.9	1.8	
Vouglans	1.8			1.8	
Val D Agri	0.2	0.1	0.2	0.2	0.3
Song Tranh A1	0.6	0.6	0.9	0.9	0.7
Song Tranh A2	0.7	0.6	1	1	0.7
Song Tranh B	0.3	1		0.8	0.3
Song Tranh C	1.1	0.7	0.8	0.8	
Song Tranh D	0.8	1	1.4	1	1
Song Tranh F	0.4	0.5	0.7	0.7	0.4

947

948

949 **Supplementary information**

950 All data in detail here and other material that provides background information are included in  
951 the file *Kostoglou\_et\_al\_supplement.docx*.